Fuzzy logic modeling of Pb (II) sorption onto mesoporous NiO/$ZnCl_2$-*Rosa Canina-L* seeds activated carbon nanocomposite prepared by ultrasound-assisted co-precipitation technique

Hamedreza Javadian, Maryam Ghasemi, Montserrat Ruiz, Ana Maria Sastre, Seyed Mostafa Hosseini Asl, Mojtaba Masomi

PII: S1350-4177(17)30376-0
DOI: http://dx.doi.org/10.1016/j.ultsonch.2017.08.022
Reference: ULTSON 3827

To appear in: *Ultrasonics Sonochemistry*

Received Date: 23 July 2017
Revised Date: 22 August 2017
Accepted Date: 22 August 2017

Please cite this article as: H. Javadian, M. Ghasemi, M. Ruiz, A.M. Sastre, S.M.H. Asl, M. Masomi, Fuzzy logic modeling of Pb (II) sorption onto mesoporous NiO/$ZnCl_2$-*Rosa Canina-L* seeds activated carbon nanocomposite prepared by ultrasound-assisted co-precipitation technique, *Ultrasonics Sonochemistry* (2017), doi: http://dx.doi.org/10.1016/j.ultsonch.2017.08.022

Fuzzy logic modeling of Pb (II) sorption onto mesoporous NiO/$ZnCl_2$-*Rosa Canina-L* seeds activated carbon nanocomposite prepared by ultrasound-assisted co-precipitation technique

Hamedreza Javadian[a,b,*], Maryam Ghasemi[b], Montserrat Ruiz[c], Ana Maria Sastre[a], Seyed Mostafa Hosseini Asl[d], Mojtaba Masomi[d]

[a]*Universitat Politècnica de Catalunya, Department of Chemical Engineering, ETSEIB, Diagonal 647, 08028 Barcelona, Spain*

[b]*Young Researchers and Elite Club, Arak Branch, Islamic Azad University, Arak, Iran*

[c]*Universitat Politècnica de Catalunya, Department of Chemical Engineering, EPSEVG, Av. Víctor Balaguer, s/n, 08800 Vilanova i la Geltrú, Spain*

[d]*Ayatollah Amoli Branch, Department of Chemical Engineering, Islamic Azad University, Amol, Iran*

[*]Corresponding author.

E-mail address: Hamedreza.javadian@yahoo.com

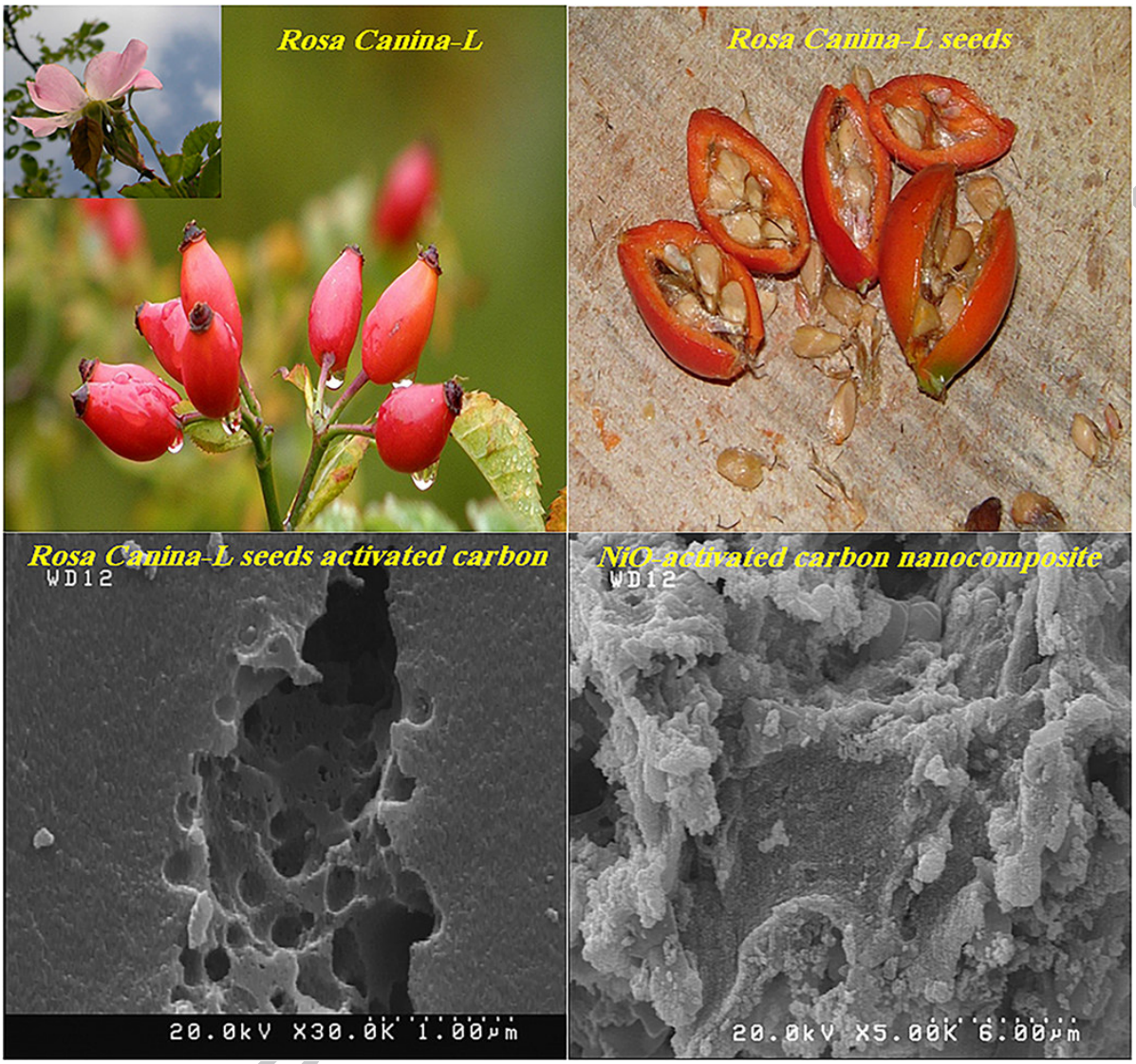

Graphical Abstract

Abstract

In this study, NiO/*Rosa Canina-L* seeds activated carbon nanocomposite (NiO/ACNC) was prepared by adding dropwise NaOH solution (2 mol/L) to raise the suspension pH to around 9 at room temperature under ultrasonic irradiation (200 W) as an efficient method and characterized by FE-SEM, FTIR and N_2 adsorption-desorption isotherm. The effect of different parameters such as contact time (0-120 min), initial metal ion concentration (25-200 mg/L), temperature (298, 318 and 333 K), amount of adsorbent (0.002-0.007 g) and the solution's initial pH (1-7) on the adsorption of Pb (II) was investigated in batch-scale experiments. The equilibrium data were well fitted by Langmuir model type 1 (R^2>0.99). The maximum monolayer adsorption capacity (q_m) of NiO/ACNC was 1428.57 mg/L. Thermodynamic parameters (ΔG°, ΔH° and ΔS°) were also calculated. The results showed that the adsorption of Pb (II) onto NiO/ACNC was feasible, spontaneous and exothermic under studied conditions. In addition, a fuzzy-logic-based model including multiple inputs and one output was developed to predict the removal efficiency of Pb (II) from aqueous solution. Four input variables including pH, contact time (min), dosage (g) and initial concentration of Pb (II) were fuzzified using an artificial intelligence-based approach. The fuzzy subsets consisted of triangular membership functions with eight levels and a total of 26 rules in the IF-THEN approach which was implemented on a Mamdani-type of fuzzy inference system. Fuzzy data exhibited small deviation with satisfactory coefficient of determination (R^2>0.98) that clearly proved very good performance of fuzzy-logic-based model in prediction of removal efficiency of Pb (II). It was confirmed that NiO/ACNC had a great potential as a novel adsorbent to remove Pb (II) from aqueous solution.

Keywords: Activated carbon, Adsorption, Fuzzy logic modeling, Kinetic, Nanocomposite, Ultrasound technique

1. Introduction

Commonly, heavy metals are present broadly in nature at natural background concentrations. Due to the mining, smelting and processing of metals, heavy metal cations such as lead, mercury, cadmium and cobalt are inserted into environments such as atmosphere, water, and soil, which cause critical environmental pollution [1]. Whereas Pb (II) has toxic effects on the living organisms, industrial effluents should be treated before discharging into environment for protection of public health and environmental surroundings [2,3].

Several methods have been used for separation of heavy metals from aqueous solutions such as reverse osmosis, pre-concentration, solvent extraction, ion exchange and adsorption. Amongst these methods, adsorption has changed to one of the most preferable methods for separation of heavy metal cations because of its high performances and cost-effectiveness [4]. In spite of possessing these features, most of adsorbents are not effective (because of diffusion limitation or the lack of enough surface active sites) or have shown problems like high cost of prices, difficulties of separation from wastewater, and generation of secondary wastes. Considering such disadvantages, recently nanoparticles have confirmed high adsorption efficiency for metal ions removal [5-8].

Previous studies found that the modification of adsorbents by loading of nanoparticles could greatly enhance the adsorption of pollutants. For example, Ghaedi et al. showed that the loading of palladium, silver and zinc oxide nanoparticles on activated carbon increased the removal of congo red from aqueous solution [5]. Gupta and Nayak found that the modification of orange peel powder with Fe_3O_4 nanoparticles increased the removal of cadmium [6]. Hashemian

and Salimi applied chemical co-precipitation method for loading $CuFe_2O_4$ on sawdust for the removal of cyanine acid blue from aqueous solution [7]. Zhang et al. modified Fe_3O_4@SiO_2 nanoparticles to attain a novel mercaptopropyl functionalized sorbent (Fe_3O_4@SiO_2-SH) by hydrolyzation of Na_2SiO_3 for the removal of mercury from aqueous solution [8].

NiO nanoparticles and several other components have illustrated unique behavior according to their size and morphology for the removal of pollutants from aqueous solutions. Therefore, studies on the synthesis of NiO nanoparticles have increased during the past decade using different methods including puttering, chemical precipitation, sol-gel, chemical vapor deposition, microwave assisted and anodic arc plasma [9]. Many researchers have done the synthesis of nanoparticles in high temperature such as Gupta and Nayak (Fe_3O_4 nanoparticles at 90 $^{\circ}$C) [6], Hashemian and Salimi (cadmium telluride nanoparticles@$CuFe_2O_4$ at 60 $^{\circ}$C) [7], Jin et al. (cetyltrimethylammonium bromide (CTAB) modified magnetic nanoparticles (Fe_3O_4@CTAB) at 80 $^{\circ}$C) [10] and Ghaedi et al. (Pd nanoparticles (Pd NPs) at 80 $^{\circ}$C, Ag nanoparticles (Ag NPs) at 50 $^{\circ}$C, ZnO nanorods (ZnO NRs) at 70 $^{\circ}$C and copper oxide on activated carbon at 75 $^{\circ}$C) [5,11]. As a promising route for preparation of various nanomaterials including metallic and ceramic particles, sonochemical methods have recently been acknowledged [12,13]. Ultrasonic irradiation has also been used for removal of metals from aqueous solution [14-16].

Utilization of multiple computational techniques for various proposes such as modeling and solving problems, has recently gained remarkable interests among researchers especially in the field of science and engineering. These soft computing techniques can precisely design and solve the dominant problems available in every process according to real operational conditions. In fact, nowadays, modeling has turned into one of the most valuable tools for

operational design and optimization of processes, examining the controlling strategies at a rational cost. Modeling not only helps to develop a comprehensive understanding of a process but also has a great potential in prediction and solving problems such as decreasing operational costs in particular processes such as adsorption process in wastewater treatment plants. The outputs of a model are a series of predicted data and can be considered as operating data providing a transparent perspective of the process in full scale [17].

Different soft computing techniques include fuzzy inference system (FIS) [18], artificial neural networks (ANN) [19], adaptive neuro-fuzzy inference system (ANFIS) [20], least square-support vector method (LS-SVM) [11], response surface methodology (RSM) [21], random forest (RF) [22], imperialist competitive algorithm (ICA) [23], firefly algorithm (FA), and genetic algorithm (GA) [24]. Among these, fuzzy logic methodology is one of the accurate and powerful modeling techniques which was successfully applied in the fields of ecology and environment for mapping, modeling, evaluation and prediction applications [25]. Fuzzy inference system was employed in prediction of removal efficiency of pollutants [26], primary warning systems [27], assessments of water quality [28], and local sustainability assessments [29]. However, there are few papers reported in literatures regarding the utilization of fuzzy logic techniques in the field of heavy metals removal from aqueous solutions and wastewaters. Rahmanian et al. [30] conducted a fuzzy modeling to predict lead removal from aqueous solution using micellar-enhanced ultrafiltration (MEUF). Therefore, fuzzy model can be used for environmental fields specifically for the prediction of adsorption process.

In this study, NiO/ACNC was synthesized by ultrasound-assisted in situ chemical precipitation technique at room temperature and characterized using FE-SEM, FTIR and N_2 adsorption-desorption isotherm. Then, the removal of Pb (II) from aqueous solution was

investigated by batch method and the uptake of metal ions onto nanocomposite was studied for determination of equilibrium, kinetic and thermodynamic parameters. Also, a Mamdani type of fuzzy inference system was applied for forecasting the removal efficiency of Pb (II) and the comparison between fuzzy and experimental data was also accomplished. The effects of four significant variables such as pH, contact time (min), adsorbent dosage (g) and initial concentration of Pb (II) (mg/L) were assessed and the importance of each factor in the process of Pb (II) adsorption on sorbent (NiO/ACNC) was obtained using sensitivity analysis.

2. Materials and methods

2.1. Materials and instruments

All chemicals and reagents used were of analytical reagent grade. Nickel nitrate hexahydrate ($Ni(NO_3)_2.6H_2O$), potassium hydroxide (KOH), zinc chloride ($ZnCl_2$) and Pb (II) nitrate hexahydrate ($Pb(NO_3)_2.6H_2O$) were purchased from Merck, Germany. The stock solution of Pb (II) (1000 mg/L) was prepared by dissolving Pb (II) nitrate hexahydrate in deionized water. The working solutions of desired concentrations were prepared by appropriate dilution of the stock solution. The initial pH of the test solutions was adjusted to the desired value, using 0.1 M HNO_3 or 0.1 M NaOH. After adsorption experiments, the supernatant liquids were filtered with Whatman #42 filter paper. The Pb (II) concentrations in the solutions were measured by a Flame Atomic Absorption Spectrometer (GBC, SensAA Dual, Australia).

2.2. Preparation of activated carbon

Activated carbon was prepared from *Rosa Canina-L* seeds obtained from Arak, Iran. After being separated from the fruit, the seeds were washed with deionized water three times in order to remove the impurities, then dried in an oven at 110 $^{\circ}$C and finally sieved to 100–120 mm. The activated carbon was prepared in the following steps [31]: 50 g of ground sample was

soaked in 50 mL concentrated solution of $ZnCl_2$ for a few hours at room temperature. After being washed with deionized water and filtrated, the sample was put in a an oven at 110 °C overnight and it was finally activated under nitrogen (N_2) atmosphere in the furnace at 400 °C for 3 h.

2.3. Preparation of NiO/ACNC

NiO/ACNC with mass ratio of 1:10 was prepared using ultrasound-assisted in situ chemical precipitation technique. The activated carbon was added into a 100 mL solution containing 0.7 mol/L nickel nitrate hexahydrate ($Ni(NO_3)_2.6H_2O$) at room temperature and stirred for 15 min. Under ultrasonic irradiation (200 W) at room temperature, NaOH solution (2 mol/L) was added dropwise to raise the suspension pH to around 9 and the irradiation was continued for 30 min. The prepared composite was repeatedly washed with deionized water, and then dried in an oven at 50 °C for 24 h and calcined at 500 °C for 4 h.

2.4. Characterization and analyses

The BET (Brunauer-Emmet-Teller) surface area was measured using N_2 adsorption at liquid nitrogen temperature (−196 °C) in Belsorp-max (Rubotherm/BEL Japan). The morphology of product was observed using a field emission scanning electron microscopy (FE-SEM) (S-4160, Hitachi, Japan). The surface chemical properties of NiO/ACNC were determined by Fourier transform infrared spectroscopy (FTIR) analysis using Shimadzu-8400s spectrometer, Japan.

2.5. Pb (II) adsorption experiments

The effect of solution pH on the adsorption of Pb (II) was investigated by adding 0.005 g of NiO/ACNC into 50 mL of Pb (II) solution. The primary concentration of ion was 100 mg/L and the mixtures were shaken for 120 min. The experiments were also done with the

various amounts of the sorbent from 0.002 to 0.007 g while the pH of the solutions was constant at optimum value. For isotherm experiments, 0.005 g of the sorbent was added into 50 mL of Pb (II) solution. The primary concentrations of ions were 25 to 200 mg/L and the mixtures were shaken at room temperature (25 $^{\circ}$C). Thermodynamic parameters were investigated at different temperatures (25, 45 and 60 $^{\circ}$C) while the primary concentration of ion was 100 mg/L. For kinetic experiments, 0.005 g of the sorbent was added to 50 mL of Pb (II) solution. The primary concentration of Pb (II) was 100 mg/L and the mixtures were shaken at different times (5-120 min). After ending contact time, samples were filtered through Whatman #42 filter paper, and then the residual concentration of Pb (II) was determined by atomic absorption spectrometer. The adsorption capacity and percentage removal of Pb (II) ion by NiO/ACNC were calculated by the bellowing equations:

$$q_e = \frac{C_0 - C_e}{m} \times V \quad (1)$$

$$\%\,\mathrm{Re}\,moval = \frac{C_0 - C_e}{C_0} \times 100 \quad (2)$$

where C_0 (mg/L) and C_e (mg/L) are the concentration of Pb (II) ion before and after adsorption tests, respectively, q_e is the adsorption capacity of Pb (II) ion, V (L) is the solution volume of Pb (II) ion, and m (g) is the amount of NiO/ACNC.

2.6. Adsorption of Pb (II)

2.6.1. Equilibrium adsorption isotherms studies

In this part of the research, the adsorption capacity of NiO/ACNC was evaluated by isotherm models such as Langmuir, Temkin, Freundlich and Dubinin Radushkevich (D-R).

Langmuir model describes quantitatively the formation of a monolayer adsorbate on the outer surface of adsorbent and after that no further adsorption takes place. It represents the

equilibrium distribution of adsorbate between the solid and liquid phases [32]. It is defined by the following equation:

$$q_e = \frac{q_m K_L C_e}{(1 + K_L C_e)} \quad (3)$$

This equation can be remodeled and rearranged into four different linear types by the following equations [33]:

Type 1 $$\frac{C_e}{q_e} = \frac{1}{q_m K_L} + \frac{C_e}{q_m} \quad (4)$$

Type 2 $$\frac{1}{q_e} = \left(\frac{1}{q_m K_L}\right)\frac{1}{C_e} + \frac{1}{q_m} \quad (5)$$

Type 3 $$q_e = q_m - \left(\frac{1}{K_L}\right)\frac{q_e}{C_e} \quad (6)$$

Type 4 $$\frac{q_e}{C_e} = K_L q_m - K_L q_e \quad (7)$$

where q_e is the adsorption capacity at equilibrium (mg/g), q_m is the maximum adsorption capacity (mg/g), C_e is the equilibrium concentration of metal ions in solution (mg/L) and K_L is Langmuir constant (L/mg). The values of isotherm constants (q_m and K_L) are defined from the slope and intercept of the linear plots of equations (4), (5), (6) and (7).

Weber and co-workers expressed the characteristic and feasibility of Langmuir isotherm in term of dimensional factor, R_L, which is defined by the following equation [34]:

$$R_L = \frac{1}{1 + K_L C_0} \quad (8)$$

Where K_L is Langmuir constant and C_0 is the initial concentration of Pb (II). The R_L value depicts the shape of the isotherm. Favorable amount of adsorption can be reached with a R_L between 0 and 1.

$R_L > 1$ Unfavorable

$R_L = 1$ Linear

$R_L < 1$ Favorable

$R_L = 0$ Irreversible

Freundlich model is an empirical relationship describing the uptake of metal ions onto a heterogeneous surface by multilayer adsorption, and assumes that different sites with several adsorption energies are involved [35]. It is expressed by the bellowing equation:

$$\log q_e = \log K_F + \frac{1}{n_F} \log C_e \quad (9)$$

where K_F is Freundlich constant (mg/g) and n_F is Freundlich exponent related to the adsorption intensity (dimensionless). The values of isotherm constants (K_F and n_F) are defined from the intercept and slope of the linear plot of ln q_e versus ln C_e, respectively. The n_F parameter, which is known as the heterogeneity factor, can be used to illustrate whether the adsorption is linear (n_F=1), a chemical process (n_F> 1) or a physical process (n_F<1). In contrast, the values of n_F<1 and n_F>1 indicate a normal Langmuir isotherm and cooperative adsorption, respectively [36].

Temkin model, which is related to the heat of adsorption of all molecules in the layer) is expressed by the bellowing equation:

$$q_e = B \ln K_T + B \ln C_e \quad (10)$$

here $B = \frac{RT}{b}$

where b and K_T are isotherm constant (J/mol) and equilibrium binding constant (L/g), respectively. The values of isotherm constants (K_T and B) are defined from the intercept and the slope of the linear plot of q_e versus ln C_e, respectively [35].

Dubinin–Radushkevich (D–R) model is also applied to estimate the porosity, free energy and the characteristics of adsorbents. D–R isotherm does not assume a homogeneous surface or constant adsorption potential [37]. D–R linear form can be shown the bellowing equation:

$$\ln q_e = \ln Q_m - K_D \varepsilon^2 \quad (11)$$

where K_D is a constant related to the adsorption energy, Q_m is the theoretical saturation capacity, and ε is the Polanyi potential, which is calculated from Eq. (12).

$$\varepsilon = RT \ln(1 + \frac{1}{C_e}) \quad (12)$$

where K_D and Q_m are isotherm constant (mol^2/kJ^2) and adsorption capacity (mg/g), respectively. The values of isotherm constants (Q_m and K_D) are defined from the intercept and slope of the linear plots of ln q_e versus ε^2, respectively. The mean free energy of adsorption (E), for transferring one mole of target from infinity in solution to the surface of the solid, is calculated from the K_D value using the bellowing equation [38]:

$$E = \frac{1}{\sqrt{2K_D}} \quad (13)$$

2.6.2. Adsorption kinetics studies

In this part of the research, the sorption procedure of Pb (II) ions onto NiO/ACNC was tested with pseudo-first-order, pseudo-second-order, intra-particle diffusion and Elovich models.

A Lagergren pseudo-first-order model is based on the assumption that the rate of adsorbate seizing the adsorption sites is proportional to the amount of untaken adsorption sites. It can be expressed by the bellowing equation:

$$\log(q_e - q_t) = \log q_e - \frac{k_1 t}{2.303} \quad (14)$$

where q_e is the adsorption capacity at equilibrium (mg/g), q_t is the adsorption capacity at the time of t (mg/g), and k_1 is first-order rate constant (1/min). The values of kinetic constants (q_e and k_1) are defined from the slope and intercept of the linear plot of log (q_e-q_t) versus t, respectively.

Pseudo-second-order model is deduced based on the hypothesis that adsorbent adsorbs the adsorbate chemically. It can be expressed by the following equation:

$$\frac{dq_t}{dt} = k_2(q_e - q_t)^2 \quad (15)$$

Eq. (15) can be linearized into four different linear types by the following equations [33]:

Type 1 $$\frac{t}{q_t} = \frac{1}{k_2 q_e^2} + \frac{1}{q_e} t \quad (16)$$

Type 2 $$\frac{1}{q_t} = \left(\frac{1}{k_2 q_e^2}\right)\left(\frac{1}{t}\right) + \frac{1}{q_e} \quad (17)$$

Type 3 $$q_t = q_e - \left(\frac{1}{k_2 q_e}\right)\frac{q_t}{t} \quad (18)$$

Type 4 $$\frac{q_t}{t} = k_2 q_e^2 - k_2 q_e q_t \quad (19)$$

where q_t is the adsorption capacity at the time of t (mg/g) and k_2 is the second order rate constant (g/(mg·min)). The values of kinetic constants (q_e and k_2) are defined from the slope and intercept of the linear plots of equations (16), (17), (18) and (19) [39].

Intra-particle diffusion model is used to identify the adsorption process of ions by the following equation [40]:

$$q_t = k_i t^{0.5} + I \quad (20)$$

where q_t is adsorption capacity at the time of t (mg/g), k_i is second-order rate constant (g/mg·min) and I indicates the thickness of the boundary layer (mg/g). The values of kinetic constants (k_i and I) are defined from the slope and intercept of the linear plot of q_t versus $t^{0.5}$, respectively.

In order to describe the adsorption procedure as a group of reaction mechanisms including diffusion in the mass of dissolution, surface diffusion and activated catalytic surfaces, Elovich model [41, 42] is applied in the following form:

$$q_t = \beta \ln(\alpha\beta) + \beta \ln t \quad (21)$$

It is postulated that Elovich constants (α and β) represent the initial adsorption rate (g/mg.min^2) and the desorption constant (mg/g.min), respectively. Elovich constants can be calculated from the plot of q_t versus ln t.

2.6.3. Adsorption thermodynamics studies

The Gibbs free energy change (ΔG^o) is an indication of spontaneity of a chemical reaction and therefore is an important criterion for spontaneity. Reactions occur spontaneously at a given temperature if ΔG^o is a negative quantity. The free energy of a sorption reaction, Enthalpy (ΔH^o) and entropy (ΔS^o) are calculated using the following equations [43]:

$$K_d = \frac{q_e}{C_e} \quad (22)$$

$$\ln K_d = \frac{\Delta S^o}{R} - \frac{\Delta H^o}{RT} \quad (23)$$

$$\Delta G^o = -RT \ln K_d \quad (24)$$

where R is the universal gas constant (8.314 J/mol.K) and T is the absolute temperature (K). By drawing a plot of ln K_d versus 1/T, the values of ΔH^o and ΔS^o are determined.

2.7. Fuzzy logic methodology

Fuzzy model is known as one of the strongest techniques to determine the input-output relation in complex nonlinear systems under uncertain and vague situations. First-time fuzzy logic model was presented by Zadeh [44] as an attempt to create systems more similar to the spirit of human thinking. The reasonable prediction of water quality is impossible for an expert using solely his mind or experience. In reality, the final result is under influence of complex environmental conditions and this problem is relevant to "principle of incompatibility" [45]. Experts' knowledge plays an important role in fuzzy model to develop a system. In a fuzzy inference system, the obtained knowledge by experts and other effective factors are defined in the format of fuzzy rules. A fuzzy inference system has three significant sections including membership functions, fuzzy set operations, and inference rules.

The precise understanding of each part is necessary in order to develop an index based on fuzzy logic. Elements of the set that present the situation are adjusted through suitable membership functions and consequently the situations of uncertainties are properly determined in fuzzy logic. The subset of membership function is composed of membership degree whose value changes between 0 and 1 (highest level) for each element [45]. Similarity rate of element x of the base set X in the fuzzy set A is expressed by the membership function $\mu_A(x)$ of x in A. The universe of discourse X is to include the dependent elements in x so that for every certain x, a set of ordered pairs is achieved by a fuzzy set A [46].

$$A = \{(x, \mu_A(x)) | x \in X\} \qquad 0 \le \mu_A(x) = 1 \tag{25}$$

There are various forms of membership functions of fuzzy sets such as triangular, trapezoidal, bell-shaped, sigmoidal, etc. The determinative factor in selecting the shape of membership functions in fuzzy models is the nature of the system [25]. One of the most prevalent membership functions used in versatile applications is the triangular shape. The advantages of triangular shape of membership functions are its simplicity in design and implementation, and also its applicability with little data [47].

There are basically two types of fuzzy inference systems, Mandani-type [48] and Takagi-Sugeno-type [49], applied for controlling and prediction of different processes. Mamdani's fuzzy inference method is the most common and applicable fuzzy methodology due to its simple representation and interpretation of fuzzy rules [50]. Fuzzy logic models utilize expert knowledge and merge them into fuzzy rules format. In the other words, a set of user-supplied rules are defined as human language in fuzzy logic model. These rules are further converted to mathematical equivalents by fuzzy systems [51]. Therefore, the most important properties of fuzzy logic models are their simplicity and flexibility. Some problems with imprecise and incomplete data and complex nonlinear functions can be solve by fuzzy logic [52].

The calculation of noisy and distorted multivariate data can be better accomplished using fuzzy logic in comparison to ANNs. Additionally, in fuzzy modeling, based on the expert knowledge, a set of fuzzy rules called rule base is established in the training phase. Interpretation of results in fuzzy model is also easier than that in ANNs [53]. Furthermore, in fuzzy model, fuzzy set operators are responsible for regulating the relationships between that fuzzy subsets. There are several fuzzy set operators useable in various fuzzy logic systems. Three basic operators are intersection (AND), union (OR), and negation (NOT) whose equations are presented below:

$$AND: \mu_{A\cap B}(x) = \mu_A(x) \bigcap \mu_B(x) = \min(\mu_A(x), \mu_B(x)) \quad (26)$$

$$OR: \mu_{A\cup B}(x) = \mu_A(x) \bigcup \mu_B(x) = \max(\mu_A(x), \mu_B(x)) \quad (27)$$

$$NOT: \mu_{\bar{A}}(x) = 1 - \mu_A(x) \quad (28)$$

The fuzzy if-then rules (fuzzy propositions) describe the relationships among the input and output in fuzzy models. In order to find the logical solution to a specific problem domain, in the absence of accurate first principle knowledge, fuzzy rules use suitable reasoning and fuzzy sets [54]. In Mamdani scheme as a type of fuzzy relational model, every fuzzy rule is defined in the format of IF-THEN relationships. Every rule is composed of two parts; the first part is an "if" that is called antecedent and the second part is "then" that is called the consequent. The structure of Mamdani models is followed by rule base. Rule base, as shown below, consists of linguistic variables like X, Y and Z:

R_i: if X is A_i and Y is B_i,. . . then Z is C_i,. . ., i = 1. . .n

In each specific input ($x_0.y_0$), the value of output Z or C is determined. The structure of model can be developed manually but the ultimate model will not change or get optimized. According to defined rules, the final performance of Mamdani fuzzy model is the production of a fuzzy membership function as an output. The approach of fuzzy model is not solely based on data set. Thus, gaining a precise result out of a generalized fuzzy model for future prediction is achievable if the adequate proficiencies are available regarding the system being investigated [55].

Generally, there are three steps in each fuzzy expert system model namely Fuzzification, inference engine (decision making logic), and defuzzification as displayed in **Fig. 1**.

3. Results and discussion

3.1. Characterization of NiO/ACNC

The FE-SEM images of the *Rosa Canina-L* seeds, prepared activated carbon and NiO/ACNC are shown in **Figs. 2 (a)** and **2 (b)**. As can be seen from these figures, the sample has a smooth surface without porous structure before activation. **Figs. 2 (c)** and **2 (d)** show a heterogeneous and porous surface that is suitable for loading of nanoparticles. It can be seen from **Fig. 3 (a)** that the surface of activated carbon is covered by a layer of NiO nanoparticles. **Fig. 3 (b)** indicates that the particles are formed homogeneous and nearly spherical, with the sizes less than 100 nm in diameter. The morphology of the nanocomposite in **Figs. 3 (c)** and **3 (d)** indicates that the agglomeration in some spots may be due to the sorption of Pb (II) ions.

Fig. 4 (a) illustrates the FTIR spectrum of NiO/ACNC. It can be confirmed that there is Ni–O band at 461.75 cm^{-1} in sample [56-58]. The main bands in the FTIR spectrum of the NiO/ACNC are at 2924.97, 1618.02, 1384.06, 1118.90, 834.23, 702.16, 570.75, 529.31 and 461.75 cm^{-1} related to aliphatic C–H groups, stretching vibration of –C–CH_2 groups, N–O nitro compound, N–H stretch, the interlayer anion (nitrate), C–H of aromatics, alkyl halides, the Fe–O vibration and Ni–O band, respectively. **Fig. 4 (b)** shows the FTIR spectrum of NiO/ACNC in the presence of Pb (II). It is clear from **Fig. 4 (b)** that after removal of Pb (II) by NiO/ACNC, the peak positions are changed or disappeared.

As far as the specific surface area and pore size distribution have an important influence on the sorption performance of sorbent, thus, N_2 adsorption–desorption isotherm of NiO/ACNC was measured at −196 $^{\circ}C$ to determine the mentioned factors. Results are shown in **Fig. 5**. It can be seen from **Fig. 5 (a)** that the adsorption-desorption isotherm of NiO/ACNC indicates a type IV isotherm including a type H3 hysteresis loop (at $p/p_0>0.4$) pursuant to the IUPAC classification [59-61]. According to this result, mesoporous structure exists in the sorbent. Pore size distribution of the sample obtained from Barrett-Joyner-Halenda [BJH] model

is shown in **Fig. 5 (b)**. The BJH pore size distribution reveals that the NiO/ACNC presents a wide pore size distribution from 1.2 to 95.2 nm with the pore diameter peaks of 1.2, 2.7, 6.05, 10.65 and 18.93. The wide pore size distribution can be useful for the penetration and adsorption of ions; therefore, the percentage removal and rate of adsorption process increase [62]. The surface area and pore analysis of NiO/ACNC are listed in **Table 1**.

3.2. Effect of solution pH and dose of NiO/ACNC

The pH of a solution can have effects on surface charge and the degree of hydrolysis of metal ions [63]. The sorption behavior of the adsorbent was investigated by change in the solution pH while other parameters such as dosage, contact time, concentration and temperature were constant. As can be seen in **Fig. 6 (a)**, by increasing the pH value from 1 to 7, the percentage removal and adsorption capacity of Pb (II) are increased from 0.04 to 91.70 % and from 0.5 to 1100.5 mg/g, respectively. At the solution pH value beyond 5 for Pb (II) ion, its removal by sorption onto sorbent along with co-precipitation or even coagulation may occur, causing the percentage removal beyond 91 % [64]. Therefore, pH=5 was chosen as an optimum pH for further experiments in this study.

An optimum adsorbent dose is needed to increase the interactions between metal ions and adsorbent sites [65]. **Fig. 6 (b)** shows the changes in percentage removal and adsorption capacity of Pb (II) by increasing the adsorbent dose from 0.002 to 0.007 g. It can be seen in **Fig. 6 (b)** that the percentage removal of Pb (II) is increased from 69.41% to 89.62% by any increase in NiO/ACNC dose, while the adsorption capacity of Pb (II) decreases from 2082.5 to 768.21 mg/g. When adsorbent dose increases, the density of reactive groups on the external surface of adsorbent for metal binding increases. Moreover, the increase in adsorbent dose may affect on concentration gradient between adsorbent surface and internal groups due to change in solution

concentration [66]. The decrease in adsorption capacity may be as a result of intrusion existing between binding sites and adsorbent, or shortage of metal ions in solution with respect to available binding sites. In addition, overlapping of sorption sites due to overcrowding of adsorbent can decrease adsorption capacity [65].

3.3. Effect of initial concentration and equilibrium adsorption isotherms

The percentage removal and adsorption capacity of Pb (II) onto NiO/ACNC at various initial concentrations from 25 to 200 mg/L are shown in **Fig. 7 (a)**. It can be seen from **Fig. 7 (a)** that the adsorption capacity increases by increasing initial concentration until it reaches to equilibrium state while the percentage removal decreases that may be due to a high collision efficiency between the metal ions and the adsorbent at lower initial concentrations and the shortage of available sites for metal ions adsorption onto sorbent surface that prevents further adsorption of metal ions at higher initial metal ion concentrations [67]. The equilibrium parameters are presented in **Table 2**. According to **Table 2** and by comparing the correlation coefficients of four isotherm models (Langmuir, Temkin, Freundlich and Dubinin-Radushkevich), it is clear that Langmuir isotherm model type 1 has the highest correlation coefficient. The maximum adsorption capacity of Pb (II) was estimated using different types of Langmuir model and found to be 1428.57, 1428.57, 1315.8 and 1383.770. It is in agreement with the reports in the literatures that used other nanoparticle adsorbents [68-70]. It can be seen from **Table 2** that the values of R_L are in the range of 0-1 (0.098, 0.091, 0.078 and 0.070 based on Langmuir isotherm models type 1, 2, 3 and 4, respectively), confirming the favorable uptake of Pb (II) ions. It is clear that the value of n is greater than 1 (2.309), indicating that the sorption intensity is favorable. The Temkin adsorption potential (B ln K_T) of NiO/ACNC is 0.103 kJ/mol

that is smaller than 8 kJ/mol, illustrating that the bond between Pb (II) and the adsorbent surface is not very strong [33]. The calculated value of adsorption free energy (E) is 0.656 kJ/mol.

3.4. Effect of contact time and adsorption kinetics

The changes in Pb (II) adsorption capacity onto NiO/ACNC at 100 mg/L initial Pb (II) concentration are presented in **Fig. 7 (b)**. As can be seen in **Fig. 7 (b)**, in the early stages of Pb (II) adsorption, the adsorption process occurs rapidly, which is probably because of the abundant availability of active sites on the adsorbent. However, the adsorption process becomes slower due to a gradual decrease in the number of active sites in the bulk of solution. The equilibrium state is achieved in a short time after a contact time of 80 min for Pb (II) adsorption.

The constants and correlation coefficients obtained from the kinetic models for Pb (II) adsorption onto NiO/ACNC are indicated in **Table 3**. By comparing the R^2 and q_e values obtained from the kinetic models, it can be mentioned that in the case of pseudo-first-order model, the R^2 values are relatively small and the experimental q_e values are in agreement with the calculated values from the linear plot, while the R^2 values are greater than 0.95 for all types of pseudo-second-order models and the values of experimental q_e and calculated q_e are very close to each other. The plot of q_t versus $t^{1/2}$ for Pb (II) adsorption by NiO/ACNC does not fit the experimental data; therefore, intra-particle diffusion is not the only rate-limiting step. The low values of correlation coefficient (R^2) for Elovich model ascertain the unsuitability of this model for Pb (II) adsorption by NiO/ACNC.

3.5. Effect of temperature and adsorption thermodynamics

The temperature dependence of Pb (II) adsorption onto NiO/ACNC is shown in **Fig. 7 (c)**. Increasing temperature from 25 to 60 $^{\circ}$C leads to a decrease in equilibrium adsorption capacity. According to Eq. (23), a plot of ln K_d versus 1/T **(Fig. 8)** is a straight line that can be used for

calculation of ΔH^o and ΔS^o. The values are listed in **Table 4**. The negative value of ΔH° (-34.098 kJ/mol) shows that the adsorption process is exothermic in nature while the positive value of ΔS^o suggests an increase in disorder at the solid–liquid interface. In addition, the negative values of ΔG° (**Table 4**) calculated from Eq. (24) confirm that Pb (II) adsorption onto NiO/ACNC is spontaneous and thermodynamically favorable.

3.6. Adsorption-desorption process

Adsorption-desorption experiments were performed three times to check the reusability of the nanocomposite. Firstly, a solution of nitric acid (HNO_3, 0.2 M) was used to desorb Pb (II) from NiO/ACNC, and then the nanocomposite was washed with deionized water to reach to neutral pH. After three cycles of adsorption–desorption, the removal efficiency of Pb (II) is shown in **Fig. 9**. As can be seen in **Fig. 9**, NiO/ACNC has a potential to be used repeatedly at least for three adsorption-desorption cycles with insignificant decrease in its removal efficiency.

3.7. Comparison with various adsorbents

The differences between the maximum monolayer adsorption capacity of NiO/ACNC and other adsorbents reported in the literatures for Pb (II) adsorption are shown in **Table 5**. As can be seen in **Table 5**, the adsorption capacity of NiO/ACNC for Pb (II) is much higher than other reported adsorbents.

3.8. Development of fuzzy model

Fuzzy logic modeling was carried out by MATLAB 2014a and developed using four input variables including pH, contact time (min), adsorbent dosage (g), and initial concentration of Pb (II) (mg/L) with ranges considered between [0, 8], [0, 120], [0, 0.008] and [0, 200], respectively. As demonstrated in **Fig. 10**, the only output variable of fuzzy model is the removal efficiency of Pb (II) (%) whose range is between [0, 100]. The membership functions determined for input

variables (pH, t, D, C) are called VVL, VL, L, LM, M, H, VH and VVH, with their names referring to "very very low", "very low", "low", "low medium", "medium", "high", "very high" and "very very high", respectively. In addition, the membership functions applied for the output variable (removal efficiency of Pb(II) (%)) are called VVL, VL, L, LM, LM1, M, M1, MH, H, VH and VVH which are the abbreviated forms of "very very low", "very low", "low", "low medium", "low medium one", "medium", "medium high", "high", "very high" and "very very high", respectively (**Fig. 10**). Triangular shape of membership functions (MFs) were chosen for all input and output variables. The similarity of membership functions in this modeling lets us follow the common mathematical definition of triangular MFs. It expresses that the triangular curve has a functional relationship with vector x, depending on three scalar parameters a, b and c:

$$f(x,a,b,c) = \begin{cases} 0 & x \le a \\ & or \\ & x \ge c \\ \frac{x-a}{b-a} & a \le x \le b \\ \frac{c-x}{c-b} & b \le x \le c \end{cases} \quad (29)$$

The above function can be changed to a compact form as in Eq. (30). The locations of parameters a and c are at the "feet" of the triangle while parameter b locates the "peak" [30].

$$f(x,a,b,c) = \max\left(\min\left(\frac{x-a}{b-a}, \frac{c-x}{c-b}\right), 0\right) \quad (30)$$

Fig. 11 is the scheme of Mamdani fuzzy inference system (FIS) applied in this study which clearly shows the performance of the model in every four steps comprising of fuzzification of the input variables, rule evaluation, aggregation of the rule outputs, and defuzzification. In the first step, the crisp inputs (numerical inputs) are taken and their degrees are determined using selected membership functions for finding suitable fuzzy sets. Further in the second step, the produced fuzzified inputs are taken and applied as the antecedent of the fuzzy rules. A fuzzy rule with

several antecedents produces a single number after antecedent evaluation using the fuzzy operators such as AND, OR and NOT. The consequent membership function is under direct influence of this number (the true value). Aggregation is the third step in which the membership functions of all rule consequents are combined into a single fuzzy set and as a result, a total output is produced. In this step, the prevalent inference methods such as max-min, max-product and sum-product are applied. The aggregation operator is demonstrated using either max or sum while the fuzzy implication operator is shown via either min or prod. Among these, the max-min inference method is known as one of the best methods in calculation of fuzzy relations with the ability of representing a computationally good and expressive setting for constraint propagation [30]. In the other words, the aggregation process is the production of one fuzzy set for each output variable using input variables consisting of the list of membership functions.

Defuzzification is the final step in fuzzy inference process where a crisp number – as an ultimate output of a fuzzy system – is produced from the aggregated output of fuzzy sets. One of the most common defuzzification methods is the centroid technique [26]. The mathematical equation of center of gravity (COG) is shown in below:

$$COG = \frac{\int \mu_A(X).xd(x)}{\int \mu_A(X).dx} \quad (31)$$

where $\mu_A(x)$ is the membership function of x in fuzzy set A.

The relationship between the input variables including pH, contact time (min), dosage (g), and initial concentration of Pb (II) (mg/L), and removal efficiency of Pb (II) (%) as the output variable was generated by 26 fuzzy model rules and consequently, three-dimensional surfaces of the fuzzy model rules were formed as illustrated in **Fig. 12**. The prediction on the removal efficiency of Pb (II) (%) as a response variable to each of the input variables was conducted using fuzzy logic model in Matlab software. As displayed in **Fig. 13**, there is a small diversion

between predicted and experimental data, clearly confirming the acceptable performance of fuzzy inference system. In addition, the correlation coefficient (R^2) of over 0.98 proves good agreement between the predicted data obtained from dynamic simulation and experimental data (**Fig. 14**). The list of all experimental and predicted data plus the full information of four input variables in each run is presented in **Table 6**. The accuracy of the predicted data gained from fuzzy model was assessed by calculating several significant parameters such as mean squared normalized error (MSE), root mean squared error (RMSE), average relative error (ARE), absolute average relative error (AARE), standard deviation (SD), and correlation coefficient (R^2). The values of MSE, RMSE, ARE, AARE, SD and R^2 were computed by fuzzy model as reported in **Table 7**. Results clearly approved the remarkable capability of the proposed fuzzy model for forecasting the removal efficiency of Pb (II). The values of MSE, RMSE, ARE, AARE, SD and R^2 were calculated using below equations:

$$MSE = \frac{1}{N}\sum_{i=1}^{n}\left(x_{Pb(II),pred} - x_{Pb(II),exp}\right)^2 \quad (32)$$

$$RMSE = \left(\frac{1}{N}\sum_{i=1}^{n}\left(x_{Pb(II),pred} - x_{Pb(II),exp}\right)^2\right)^2 \quad (33)$$

$$ARE = \frac{1}{N}\sum_{i=1}^{N}\left(\frac{X_{exp\,(i)} - X_{pred(i)}}{X_{exp(i)}}\right) \quad (34)$$

$$AARE = \frac{1}{N}\sum_{i=1}^{N}\left(\left|\frac{X_{exp(i)} - X_{pred(i)}}{X_{exp(i)}}\right|\right) \quad (35)$$

$$SD = \sqrt{\frac{1}{N-1}\sum_{i=1}^{n}\left(\left|\frac{X_{exp(i)}-X_{pred(i)}}{X_{exp(i)}}\right| - AARE\right)^2} \quad (36)$$

$$R^2 = \frac{(\sum_{i=1}^{n}(x_{Pb(II),exp}-\overline{x_{Pb(II),exp}})(x_{Pb(II),pred}-\overline{x_{Pb(II),pred}}))^2}{\sum_{i=1}^{n}(x_{Pb(II),exp}-\overline{x_{Pb(II),exp}})^2(x_{Pb(II),pred}-\overline{x_{Pb(II),pred}})^2} \quad (37)$$

Also, the fuzzy model used in this work was compared with other relevant models applied in previous studies in the field of pollutions removal from queues solutions. **Table 8** indicates the summery of information including type of adsorbent and the predicted results of various models employed in adsorption process. The evaluations demonstrate that the developed statistical model used in this study had reasonably precise performance in comparison to other models. Briefly, the fuzzy logic model effectively detected the complex non-linear relationships between important variables existing in adsorption process.

3.9. Sensitivity analysis

In order to evaluate the relative importance of each input parameters on the output variable of fuzzy model, a sensitivity analysis was carried out. This analysis was done separately for each input variable in a way that one input parameter was changed in equal intervals of a given point while the other input variables were kept constant. It was observed that the rate of changes for every input parameter rather than the output variable was different (**Fig. 15**). In comparison to the other three assessed input variables, pH of aqueous solution showed higher effectiveness on removal efficiency of Pb (II). As indicated in **Fig. 15**, the sensitivity of removal efficiency (R %) rather than contact time (min) had the lowest amount (3.51%) compared to the other variables of the adsorption process. This can be easily interpreted through the time curve versus removal efficiency. A considerable part of the adsorption was carried out in the first 60 minutes (steep

slope) and thereafter, particularly in the range of experiments, the amount of adsorption growth was low (mild slope).

4. Conclusions

NiO/*Rosa Canina-L* seeds activated carbon nanocomposite was successfully synthesized by ultrasound-assisted in situ chemical precipitation technique and characterized using FE-SEM, FTIR and N_2 adsorption-desorption isotherm. The effect of some factors such as solution pH, amount of adsorbent, contact time, initial metal ions concentration and temperature on adsorption efficiency was investigated by batch method. The equilibrium data were well fitted by Langmuir isotherm type 1, and Pb (II) adsorption capacity onto NiO/ACNC was 1428.57 mg/g. Pb (II) adsorption was rapid within 30 min of contact time. The kinetic of Pb (II) adsorption onto NiO/ACNC was based on the assumption of pseudo-second-order model type 1. Thermodynamic parameters showed that Pb (II) adsorption onto NiO/ACNC was feasible, spontaneous and exothermic. According to the experimental data, a Mamdani type of fuzzy inference system was developed by means of 26 if-then rules, and applied to forecast the removal performance of sorbent. Results showed that the proposed fuzzy logic model favorably predicted the removal efficiency of Pb (II) with correlation coefficient of over 0.98. We suggest that extra input and output variables be considered to reach a more realistic prediction of removal efficiency of Pb (II). Also, a mixture of different membership functions (MFs) can be used in proposed fuzzy logic based model for increasing the accuracy of prediction. Based on the experimental and predicted data, NiO/ACNC can be used as an effective adsorbent for Pb (II) adsorption from aqueous solution.

Acknowledgements

This work has been supported by the Spanish Ministry of Economy and Competitiveness (Ref. CTM2014-52770-R). Hamedreza Javadian acknowledges the financial support received (Ref. BES-2015-072506).

References

[1] Abdelhafez Ahmed A, Li J. Removal of Pb (II) from aqueous solution by using biochars derived from sugar cane bagasse and orange peel. J. Taiwan. Inst. Chem. Eng. 2016; 61:367-75.

[2] Fu R, Liu Y, Lou Z, Wang Z, Baig SA, Xu X. Adsorptive removal of Pb (II) by magnetic activated carbon incorporated with amino groups from aqueous solutions. J. Taiwan. Inst. Chem. Eng. 2016; 62:247-58.

[3] Shojaeipoor F, Elhamifar D, Moshkelgosha R, Masoumia B. Removal of Pb (II) and Co (II) ions from aqueous solution and industrial wastewater using ILNO-NH_2: Kinetic, isotherm and thermodynamic studies. J. Taiwan. Inst. Chem. Eng. 2016; 67:166-73.

[4] Soliman AM, Elwy HM, Thiemann T, Majedi Y, Labata FT, Al-Rawashdeh NAF. Removal of Pb (II) ions from aqueous solutions by sulphuric acid-treated palm tree leaves. J. Taiwan. Inst. Chem. Eng. 2016; 58:264-73.

[5] Ghaedi M, Nejati Biyareh M, Nasiri Kokhdan S, Shamsaldini S, Sahraei R, Daneshfar A, Shahriyar S. Comparison of the efficiency of palladium and silver nanoparticles loaded on activated carbon and zinc oxide nanorods loaded on activated carbon as new adsorbents for removal of Congo red from aqueous solution: Kinetic and isotherm study. Mater. Sci. Eng. 2012; 32:725-34.

[6] Gupta VK, Nayak A. Cadmium removal and recovery from aqueous solutions by novel adsorbents prepared from orange peel and Fe_2O_3 nanoparticles. Chem. Eng. J. 2012; 180:81–90.

[7] Hashemian S, Salimi M. Nano composite a potential low cost adsorbent for removal of cyanine acid. Chem. Eng. J. 2012; 188:57-63.

[8] Zhang S, Zhang Y, Liu J, Xu Q, Xiao H, Wang X, Xu H, Zhou J. Thiol modified Fe_3O_4@SiO_2 as a robust, high effective, and recycling magnetic sorbent for mercury removal. Chem. Eng. J. 2013; 226:30-8.

[9] Kwak B S, Choi B H, Ji M J, Park S M, Kang M. Synthesis of spherical NiO nanoparticles using a solvothermal treatment with acetone solvent. J. Ind. Eng. Chem. 2012; 18:11-5.

[10] Jin Y, Liu F, Tong M, Hou Y. Removal of Arsenate by cetyltrimethylammonium bromide modified magnetic nanoparticles. J. Hazard. Mater. 2012; 227-228:461-8.

[11] Ghaedi M, Ghaedi A M, Hossainpour M, Ansari A, Habibi M H, Asghari A R. Least square-support vector (LS-SVM) method for modeling of methylene blue dye adsorption using copper oxide loaded on activated carbon: Kinetic and isotherm study. J. Ind. Eng. Chem. 2014; 25:1641-9.

[12] Arami H, Mazloumi M, Khalifehzadeh R, Sadrnezhaad SK. Sonochemical preparation of TiO_2 nanoparticles. Mater. Lett. 2007; 61:4559-61.

[13] Neppolian B, Wang Q, Jung H, Choi H. Ultrasonic-assisted sol–gel method of preparation of TiO_2, nano-particles: characterization, properties and 4-chlorophenol removal application. Ultrason. Sonochem. 2008; 15:649-58.

[14] Saad M, Tahir H, Ali D. Green synthesis of Ag-Cr-AC nanocomposites by Azadirachta indica and its application for the simultaneous removal of binary mixture of dyes by ultrasonicated assisted adsorption process using Response Surface Methodology. Ultrason. Sonochem. 2017; 38:197-213.

[15] Saad M, Tahir H. Synthesis of carbon loaded γ-Fe_2O_3 nanocomposite and their applicability for the selective removal of binary mixture of dyes by ultrasonic adsorption based on response surface methodology. Ultrason. Sonochem. 2017; 36:393-408.

[16] Saad M, Tahir H, Khan J, Hameed U, Saud A. Synthesis of polyaniline nanoparticles and their application for the removal of Crystal Violet dye by ultrasonicated adsorption process based on Response Surface Methodology. Ultrason. Sonochem. 2017; 34:600-8.

[17] Yetilmezsoy K. A new empirical model for the determination of the required retention time in hindered settling, Fresenius Environ. Bull. 2007; 16:674-84.

[18] Ghaedi A, Vafaei A, Mohagheghian M, Afshar N, Hafezi S. Fuzzy modelling of concentration in chamomile solution using reverse osmosis, Fresenius Environ. Bull. 2012; 21: 634-43.

[19] Hosseini Asl S M, Ahmadi M, Ghiasvand M, Tardast A, Katal R. Artificial neural network (ANN) approach for modeling of Cr(VI) adsorption from aqueous solution by zeolite prepared from raw fly ash (ZFA), J. Ind. Eng. Chem. 2013; 19:1044-55.

[20] Ghaedi M, Hosaininia R, Ghaedi A, Vafaei A, Taghizadeh F. Adaptive neuro-fuzzy inference system model for adsorption of 1,3,4-thiadiazole-2,5-dithiol onto gold nanoparticales-activated carbon, Spectrochim. Acta A: Mol. Biomol. Spectrosc. 2014; 131:606-14.

[21] Hajati S, Ghaedi M, Mazaheri H. Removal of methylene blue from aqueous solution by walnut carbon: optimization using response surface methodology, Desalin. Water Treat. 2014; 52:1-15.

[22] Ghaedi M, Ghaedi A M, Negintaji E, Ansari A, Vafaei A, Rajabi M. Random forest model for removal of bromophenol blue using activated carbon obtained from Astragalus bisulcatus tree, J. Ind. Eng. Chem. 2014; 20:1793-1803.

[23] Ghaedi M, Ghaedi A M, Negintaji E, Ansari A, Mohammadi F. Artificial neural network-Imperialist competitive algorithm based optimization for removal of sunset yellow using $Zn(OH)_2$ nanoparticles-activated carbon, J. Ind. Eng. Chem. 2014; 20:4332-43.

[24] Ghaedi M, Zeinali N, Ghaedi A M, Teimuori M, Tashkhourian J. Artificial neural network-genetic algorithm based optimization for the adsorption of methylene blue and brilliant green from aqueous solution by graphite oxide nanoparticle, Spectrochim. Acta. A: Mol. Biomol. Spectrosc. 2014; 125: 264-77.

[25] Metternicht G, Gonzalez S. FUERO: foundations of a fuzzy exploratory model for soil erosion hazard prediction, Environ. Model. Softw. 2005; 20:715-28.

[26] Kotti I P, Sylaios G K, Tsihrintzis V A. Fuzzy logic models for BOD removal prediction in free-water surface constructed wetlands, Ecol. Eng. 2013; 51:66-74.

[27] Dokas I M, Karras D A, Panagiotakopoulos D C. Fault tree analysis and fuzzy expert systems: Early warning and emergency response of landfill operations, Environ. Model. Softw. 2009; 24:8-25.

[28] Gharibi H, Mahvi A H, Nabizadeh R, Arabalibeik H, Yunesian M, Sowlat M H. A novel approach in water quality assessment based on fuzzy logic, J. Environ. Manage. 2012; 112: 87-95.

[29] Canavese D, Ortega N R S, Queirós M. The assessment of local sustainability using fuzzy logic: An expertopinion system to evaluate environmental sanitation in the Algarveregion, Portugal, Ecol. Indic. 2014; 36:711-8.

[30] Rahmanian B, Pakizeh M, Esfandyari M, Heshmatnezhad F, Maskooki A. Fuzzy modeling and simulation for lead removal using micellar-enhanced ultrafiltration (MEUF), J. Hazard. Mater. 2011; 192:585- 92.

[31] Cheng J Y, Yang L, Dong L, Long X L, Yuan W K. Regeneration of hexamminecobalt(II) under the catalysis of activated carbon modified with $ZnCl_2$ solution. J. Ind. Eng. Chem. 2012; 18:1628-34.

[32] Javadian H, Ghorbani F, Tayebi H, Hosseini Asl S M. Study of the adsorption of Cd (II) from aqueous solution using zeolite-based geopolymer, synthesized from coal fly ash; kinetic, isotherm and thermodynamic studies. Arab. J. Chem. 2015; 8:837-49.

[33] Asgari G, Roshani B, Ghanizadeh G. The investigation of kinetic and isotherm of fluoride adsorption onto functionalize pumice stone. J. Hazard. Mater. 2012; 217-218:123-32.

[34] Javadian H, Vahedian P and Toosi M, Adsorption characteristics of Ni(II) from aqueous solution and industrial wastewater onto Polyaniline/HMS nanocomposite powder. Appl. Surf. Sci. 2013; 284:13-22.

[35] Javadian H, Taghavi M. Application of novel Polypyrrole/thiol-functionalized zeolite Beta/MCM-41 type mesoporous silica nanocomposite for adsorption of Hg^{2+} from aqueous solution and industrial wastewater: Kinetic, isotherm and thermodynamic studies. Appl. Surf. Sci. 2014; 289:487-94.

[36] Wang L. Application of activated carbon derived from ‘waste’ bamboo culms for theadsorption of azo disperse dye: Kinetic, equilibrium and thermodynamic studies. J Environ Manage 2012; 102:79-87.

[37] Javadian H, Ahmadi M, Ghiasvand M, Kahrizi S, Katal R. Removal of Cr (VI) by modified brown algae *Sargassum bevanom* from aqueous solution and industrial wastewater. J. Taiwan Ins. Chem. Eng. 2013; 44:977-89.

[38] Javadian H, Zamani Sorkhrodi F, Babzadeh Koutenaei B. Experimental investigation on enhancing aqueous cadmium removal via nanostructure composite of modified hexagonal type

mesoporous silica with polyaniline/polypyrrole nanoparticles. J. Ind. Eng. Chem. 2014; 20:3678-88.

[39] Javadian H. Adsorption performance of suitable nanostructured novel composite adsorbent of poly(N-methylaniline) for removal of heavy metal from aqueous solutions. J. Ind. Eng. Chem. 2014; 20:4344-52.

[40] Javadian H. Application of kinetic, isotherm and thermodynamic models for the adsorption of Co (II) ions on polyaniline/polypyrrole copolymer nanofibers from aqueous solution. J. Ind. Eng. Chem. 2014; 20:4233-41.

[41] Ghasemi M, Naushad M, Ghasemi N, Khosravi-fard Y. Adsorption of Pb (II) from aqueous solution using new adsorbents prepared from agricultural waste: Adsorption isotherm and kinetic studies. J. Ind. Eng. Chem. 2014; 20:2193-9.

[42] Javadian H, Torabi Angaji M, Naushad M. Synthesis and characterization of polyaniline/γ-alumina nanocomposite: A comparative study for the adsorption of three different anionic dyes. J. Ind. Eng. Chem. 2014; 20:3890-900.

[43] Ghasemi M, Zeinaly Khosroshahy M, Bavand Abbasabadi A, Ghasemi N, Javadian H, Fattahi M. Microwave-assisted functionalization of *Rosa Canina-L* fruits activated carbon with tetraethylenepentamine and its adsorption behavior toward Ni (II) in aqueous solution: Kinetic, equilibrium and thermodynamic studies. Powder Technol. 2015; 274:362-71.

[44] Zadeh, L. Outline of a new approach to the analysis of complex systems and decision processes. IEEE Trans. Syst. Man. Cybern. 1973; 3:28-44.

[45] Topcu I B, Saridemir M. Prediction of rubberized concrete properties using artificial neural network and fuzzy logic, Construct. Build. Mater. 2008; 22:532-40.

[46] Ocampo-Duque W, Ferré-Huguet, N, Domingo, J L, Schuhmacher M. Assessing water quality in rivers with fuzzy inference systems: a case study, Environ. Int. 2006; 32:733-42.

[47] Aydinol F, Yetilmezsoy K. A fuzzy-logic-based model to predict biogas and methane production rates in a pilot-scale mesophilic UASB reactor treating molasses wastewater, J. Hazard. Mater. 2010; 182:460-71.

[48] Mamdani E H, Assilian S. An experiment in linguistic synthesis of fuzzy controllers, Int. J. Man-Mach. Stud. 1975; 7:1-13.

[49] Takagi T, Sugeno M. Fuzzy identification of systems and its application to modeling and control, IEEE Trans. Syst. Man Cyber. 1985; 15:116-32.

[50] Acaroglu O, Ozdemir L. Asbury B. A fuzzy logic model to predict specific energy requirement for TBM performance prediction, Tunnel. Under. Space Technol. 2008; 23:600-8.

[51] Sadrzadeh M. Ghadimi A, Mohammadi T. Coupling a mathematical and a fuzzy logic-based model for prediction of zinc ions separation from wastewater using electrodialysis, Chem. Eng. J. 2009; 15:262-74.

[52] L.A. Zadeh. Making computer think like people, IEEE Spectr. 1984; 8:26-32.

[53] Altunkaynak A, Chellam S. Prediction of specific permeate flux during cross flow microfiltration of polydispersed colloidal suspensions by fuzzy logic models, Desalination, 2010; 253:188-94.

[54] Alvarez Grima M. BabusIka R. Fuzzy model for the prediction of unconfined compressive strength of rock samples, Int. J. Rock Mech. Min. Sci. 1999; 36:339-49.

[55] Keshwani D R, Jones D D, Meyer G E. Brand R M. Rule-based Mamdani-type fuzzy modeling of skin permeability, Appl. Soft Comput. 2008; 8:285-94.

[56] Aghazadeh M, Nozad Golikand A. Ghaemi M, Synthesis, characterization, and electrochemical properties of ultrafine b-$Ni(OH)_2$ nanoparticles. Int. J. Hydrogen Energy 2011; 36:8674-9.

[57] Biju V, Abdul Khadar M. Fourier transform infrared spectroscopy study of nanostructured nickel oxide. Spectrochim. Acta. Part A 2003; 59:121-34.

[58] Yeganeh Ghotbi M. Nickel doped zinc oxide nanoparticles produced by hydrothermal decomposition of nickel-doped zinc hydroxide nitrate. Particuology 2012; 10:492-6.

[59] Sun G, Zhang S, Li Y. Solvothermal synthesis of Zn_2SnO_4 nanocrystals and their photocatalytic properties, Int. J. Photoenergy 2014, http://dx.doi.org/10.1155/2014/580615

[60] Yuan J J, Zhu P X, Noda D, Jin R H. Controlled synthesis and tunable properties of ultrathin silica nanotubes through spontaneous polycondensation on polyamine fibrils. Beilstein J. Nanotechnol. 2013; 4:793-804.

[61] Wang C, Le Y, Cheng B. Fabrication of porous ZrO_2 hollow sphere and its adsorption performance to Congo red in water. Ceram. Int. 2014; 40:10847-56.

[62] Fan J J, Cai W Q, Yu J G. Adsorption of N719 dye on anatase TiO_2 nanoparticles and nanosheets with exposed (001) facets: equilibrium, kinetic, and thermodynamic studies. Chem. Asian J. 2011;6: 2481-90.

[63] Ghaedi M, Montazerozohori M, Sajedi M, Roosta M, Nickoosiar Jahromi M, Asghari A. Comparison of novel sorbents for preconcentration of metal ions prior to their flame atomic absorption spectrometry determination. J. Ind. Eng. Chem. 2013; 19:1781-7.

[64] Lee S M, Laldawngliana C, Tiwari D. Iron oxide nano-particles-immobilized-sand material in the treatment of Cu(II), Cd(II) and Pb(II) contaminated waste waters. Chem. Engin. J. 2012; 195-196:103-11.

[65] Xu P, Zeng G, Huang D, Hua S, Feng C, Lai C, Zhao M, Huang C, Li N, Wei Z, Xie G. Synthesis of iron oxide nanoparticles and their application in *Phanerochaete chrysosporium* immobilization for Pb (II) removal. Colloids Surf A Physicochem. Eng. Aspects 2013; 419:147-55.

[66] Boschi C, Maldonado H, Ly M, Guibal E. Cd (II) biosorption using *Lessonia* kelps, J. Colloid Interface Sci. 2011; 357:487-96.

[67] Ma X, Li L, Yang L, Su C, Wang K, Yuan S, Zhou J. Adsorption of heavy metal ions using hierarchical $CaCO_3$–maltosemeso/macroporous hybrid materials: Adsorption isotherms and kinetic studies. J. Hazard. Mater. 2012; 209-210:467-77.

[68] Idris A, Suriani Mohd Ismail N, Hassan N, Misran E, Ngomsik A F. Synthesis of magnetic alginate beads based on maghemite nanoparticles for Pb (II) removal in aqueous solution. J. Ind. Eng. Chem. 2012; 18:1582-9.

[69] Tan Y, Chen M, Hao Y. High efficient removal of Pb (II) by amino-functionalized Fe_3O_4 magnetic nano-particles. Chem. Eng. J. 2012; 191:104-11.

[70] Ge F, Li M M, Ye H, Zhao B X. Effective removal of heavy metal ions Cd^{2+}, Zn^{2+}, Pb^{2+}, Cu^{2+} from aqueous solution by polymer-modified magnetic nanoparticles. J. Hazard. Mater. 2012; 211- 212:366-72.

[71] Wang T, Jin X, Chen Z, Megharaj M, Naidu R. Simultaneous removal of Pb (II) and Cr (III) by magnetite nanoparticles using various synthesis conditions. J. Ind. Eng. Chem. 2014; 20:3543-9.

[72] Vinh Tran H, Dai Tran L, Ngoc Nguyen T. Preparation of chitosan/magnetite composite beads and their application for removal of Pb (II) and Ni (II) from aqueous solution. Mater. Sci. Eng. C 2010; 30:304-10.

[73] Jabeen H, Kemp K C, Chandra V. Synthesis of nano zerovalent iron nanoparticles-Graphene composite for the treatment of lead contaminated water. J. Environ. Manage. 2013; 130:429-35.

[74] Zhang J, Zhai S, Li S, Xiao Z., Song Y, An Q, Tian G. Pb (II) removal of Fe_3O_4@SiO_2-NH_2 core-shell nanomaterials prepared via a controllable sol-gel process. Chem. Eng. J. 2013; 215-216:461-71.

[75] Xu P, Zeng G M, Huang D L, Lai C, Zhao M H, Wei Z, Li N J, Huang C, Xie G X. Adsorption of Pb (II) by iron oxide nanoparticles immobilized *Phanerochaete chrysosporium*: Equilibrium, kinetic, thermodynamic and mechanisms analysis. Chem. Eng. J. 2012; 203:423-31.

[76] Xin X, Wei Q, Yang J, Yan L, Feng R, Chen G, Du B, Li H. Highly efficient removal of heavy metal ions by amine-functionalized mesoporous Fe_3O_4 nanoparticles. Chem. Eng. J. 2012; 184:132-40.

[77] Fatyasari Nata I, Wijaya Salim G, Lee C K. Facile preparation of magnetic carbonaceous nanoparticles for Pb^{2+} ions removal, J. Hazard. Mater. 2010; 183:853-8.

[78] Nassar N N. Rapid removal and recovery of Pb (II) from wastewater by magnetic nano adsorbents, J. Hazard. Mater. 2010; 184:538-46.

[79] Fotoohi F, Iranagh S. A, Golzar K, Modarress H. Predicting pure and binary gas adsorption on activated carbon with two-dimensional cubic equations of state (2-D EOSs) and artificial neural network (ANN) method, Phys. Chem. Liq. 2016; 54:281-302.

[80] Ghaedi M, Ansari A, Bahari F, Ghaedi A M, Vafaei A. A hybrid artificial neural network and particle swarm optimization for prediction of removal of hazardous dye brilliant green from aqueous solution using zinc sulfide nanoparticle loaded on activated carbon. Spectrochim. Acta Part A, 2015; 137:1004-15.

[81] Ghaedi A M, Ghaedi M, Karami P. Comparison of ultrasonic with stirrer performance for removal of sunset yellow (SY) by activated carbon prepared from wood of orange tree: Artificial neural network modeling. Spectrochim. Acta Part A, 2015; 138:789-99.

[82] Jamshidi M, Ghaedi M, Dashtian K, Ghaedi A M, Hajati S, Goudarzi A, Alipanahpour E. Highly efficient simultaneous ultrasonic assisted adsorption of brilliant green and eosin B onto ZnS nanoparticles loaded activated carbon: Artificial neural network modeling and central composite design optimization. Spectrochim. Acta Part A, 2016; 153:257-67.

[83] Ghaedi M, Shojaeipour E, Ghaedi A M, Sahraei R. Isotherm and kinetics study of malachite green adsorption onto copper nanowires loaded on activated carbon: Artificial neural network modeling and genetic algorithm optimization. Spectrochim. Acta Part A, 2015; 142:135-49.

[84] Noorimotlagh Z, Shahriyar S, Darvishi Cheshmeh Soltani R, Tajik R. Optimized adsorption of 4-chlorophenol onto activated carbon derived from milk vetch utilizing response surface methodology, Desalin. Water Treat. 2016; 30:14213-26.

[85] Mohammadzadeh A, Ramezani M, Ghaedi A M. Synthesis and characterization of Fe_2O_3-ZnO-$ZnFe_2O_4$/carbon nanocomposite and its application to removal of bromophenol blue dye using ultrasonic assisted method: Optimization by response surface methodology and genetic algorithm, J. Taiwan Inst. Chem. Eng. 2016; 59:275-84.

[86] Dehghanian N, Ghaedi M, Ansari A, Ghaedi A, Vafaei A, Asif M, Agarwal S, Tyagi I, Gupta VK. A random forest approach for predicting the removal of Congo red from aqueous solutions by adsorption onto tin sulfide nanoparticles loaded on activated carbon, Desalin. Water Treat. 2016; 20:9272-85.

[87] Mahmoodi N M, Chamani H, Kariminia H R. Functionalized copper oxide–zinc oxide nanocomposite: synthesis and genetic programming model of dye adsorption, Desalin. Water Treat. 2016; 40:18755-69.

Caption for the figures

Fig. 1. Fuzzy inference system.

Fig. 2. FE-SEM image of (a) crushed *Rosa Canina-L* seeds (b) crushed *Rosa Canina-L* seeds with more zoom (c) after activation of *Rosa Canina-L* seeds (d) after activation of *Rosa Canina-L* seeds with more zoom.

Fig. 3. FE-SEM image of (a) NiO/ACNC (b) NiO/ACNC with more zoom (c) Pb (II)-NiO/ACNC (d) Pb (II)-NiO/ACNC with more zoom.

Fig. 4. FTIR spectrum of (a) NiO/ACNC before adsorption and (b) NiO/ACNC after adsorption.

Fig. 5. (a) N_2 adsorption-desorption isotherm of NiO/ACNC and (b) BJH plot of NiO/ACNC.

Fig. 6. (a) Effect of pH on Pb (II) adsorption by NiO/ACNC (b) Effect of adsorbent dose on Pb (II) adsorption by NiO/ACNC.

Fig. 7. (a) Effect of initial concentration on Pb (II) adsorption by NiO/ACNC (b) Effect of contact time on Pb (II) adsorption by NiO/ACNC (c) Effect of temperature on Pb (II) adsorption by NiO/ACNC.

Fig. 8. Ln K_d versus 1/T for determination of enthalpy and entropy changes of the sorption process.

Fig. 9. Adsorption-desorption process.

Fig. 10. Fuzzy membership functions of input and output variables (pH, contact time (min), adsorbent dosage (g), initial concentration of Pb (II) (mg/L) and Pb (II) removal efficiency (%)).

Fig. 11. Input-output map of fuzzy inference system (FIS) modeled for prediction of Pb (II) removal efficiency (%).

Fig. 12. Three dimentional surfaces of fuzzy model rules for Pb (II) removal efficiency (%).

Fig. 13. Response of fuzzy inference model; the effect of (a) pH, (b) contact time (min), (C) adsorbent dosage (g) and (d) initial concentration of Pb (II) (mg/L) on Pb (II) removal efficiency (%).

Fig. 14. Comparison between the experimental data of Pb (II) removal efficiency (%) and the predicted data using fuzzy inference model.

Fig. 15. Relative importance of each input parameter on Pb (II) removal efficiency.

Fig. 1

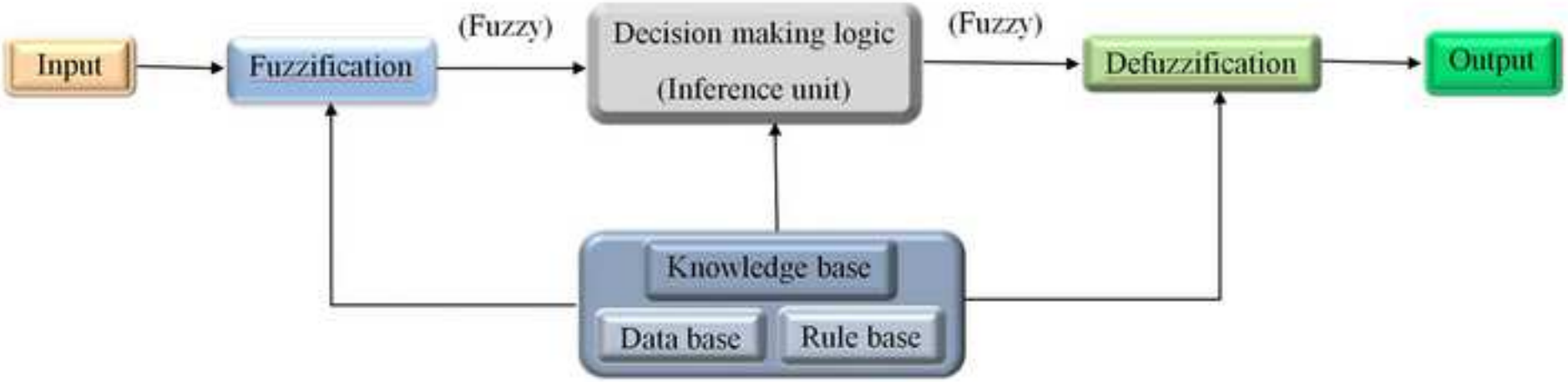

Fig. 2

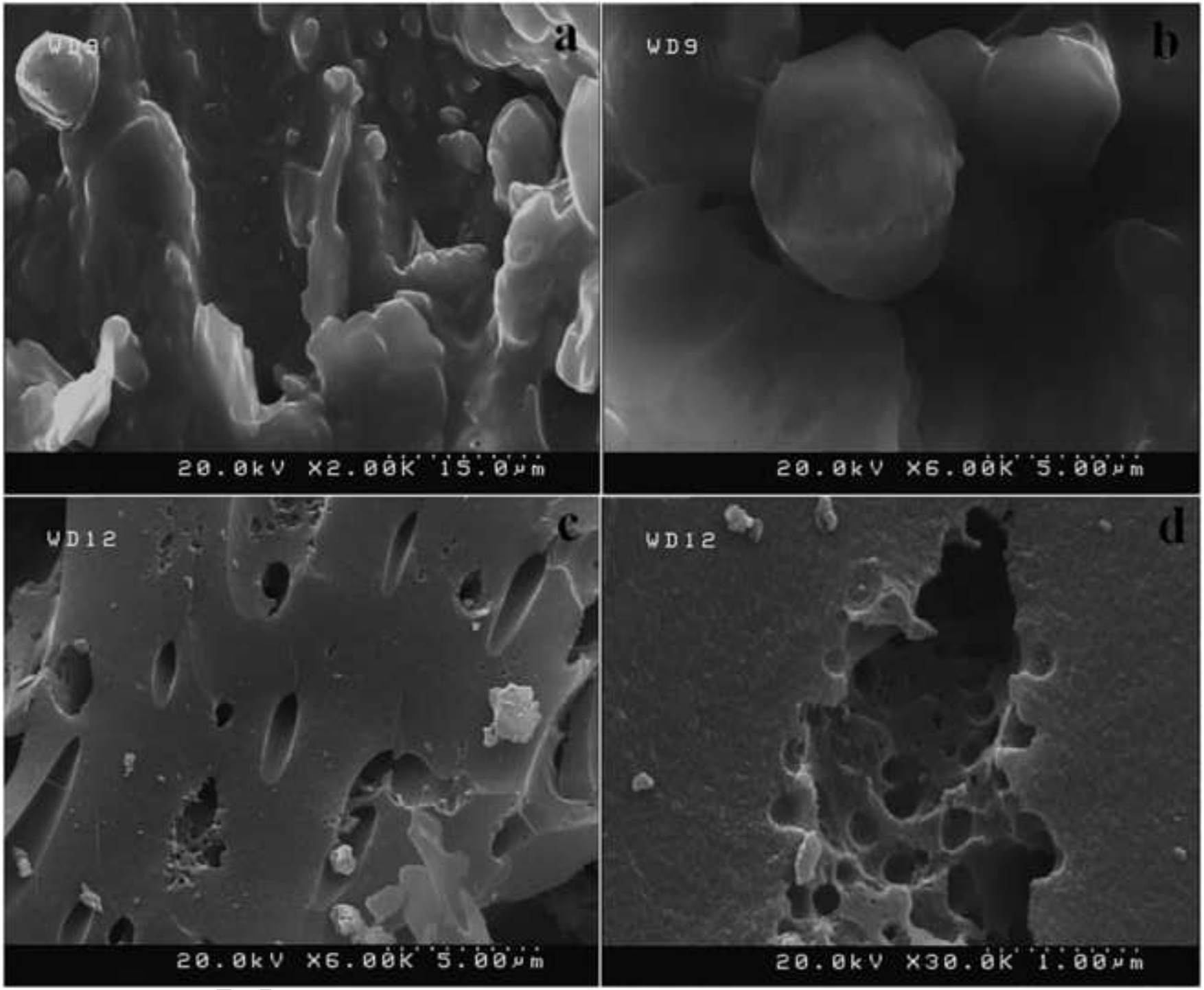

Fig. 3

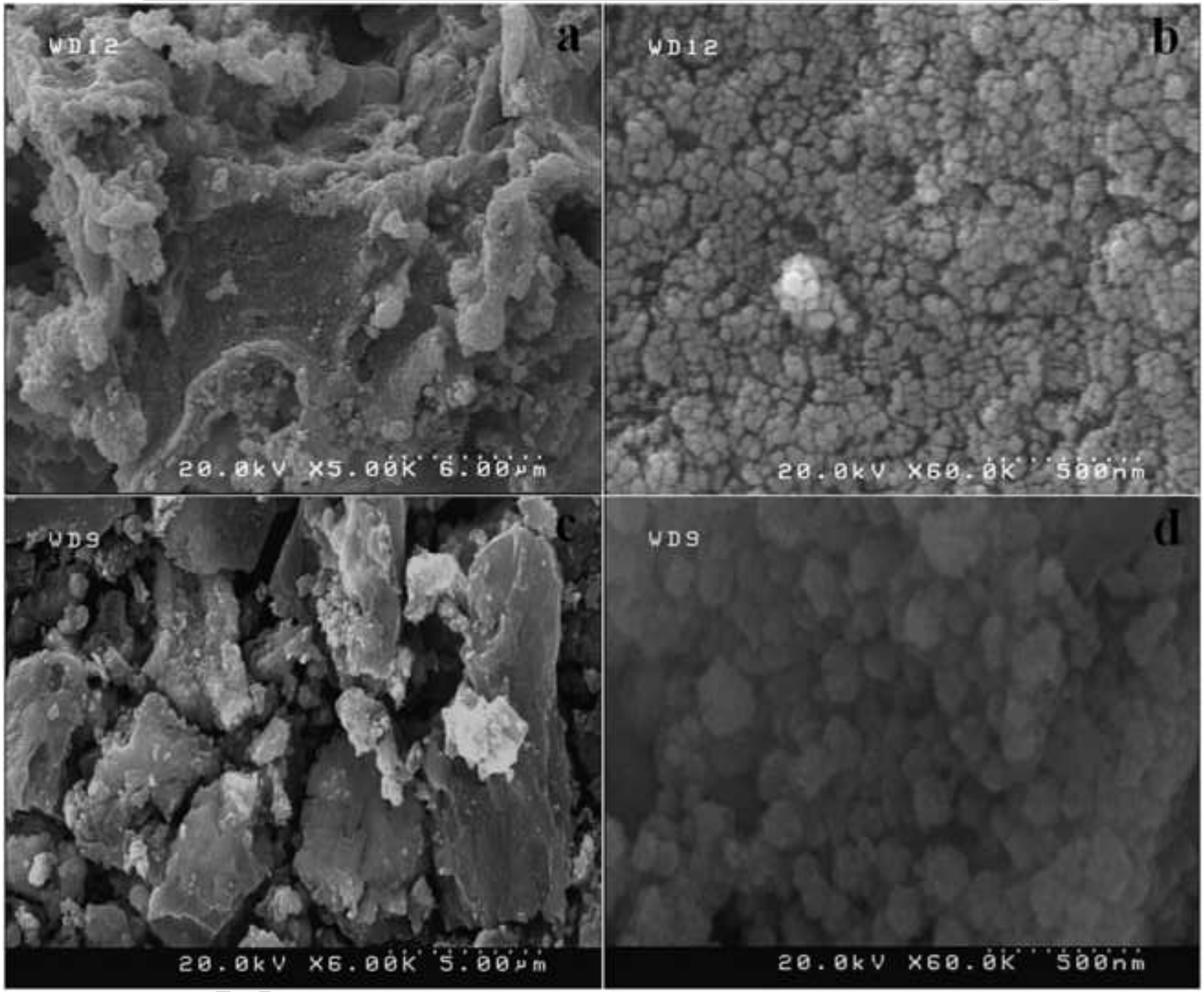

Fig. 4

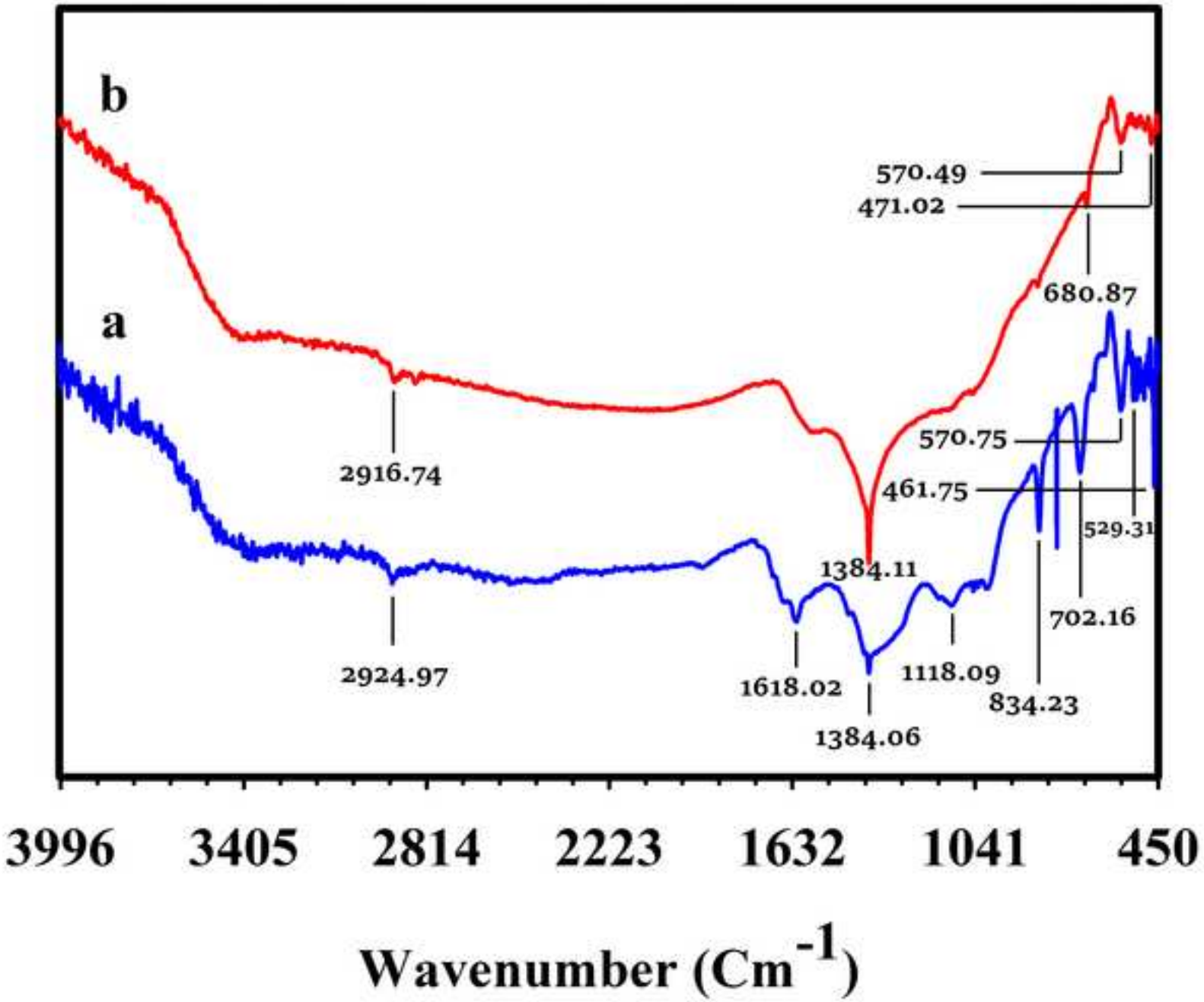

Fig. 5

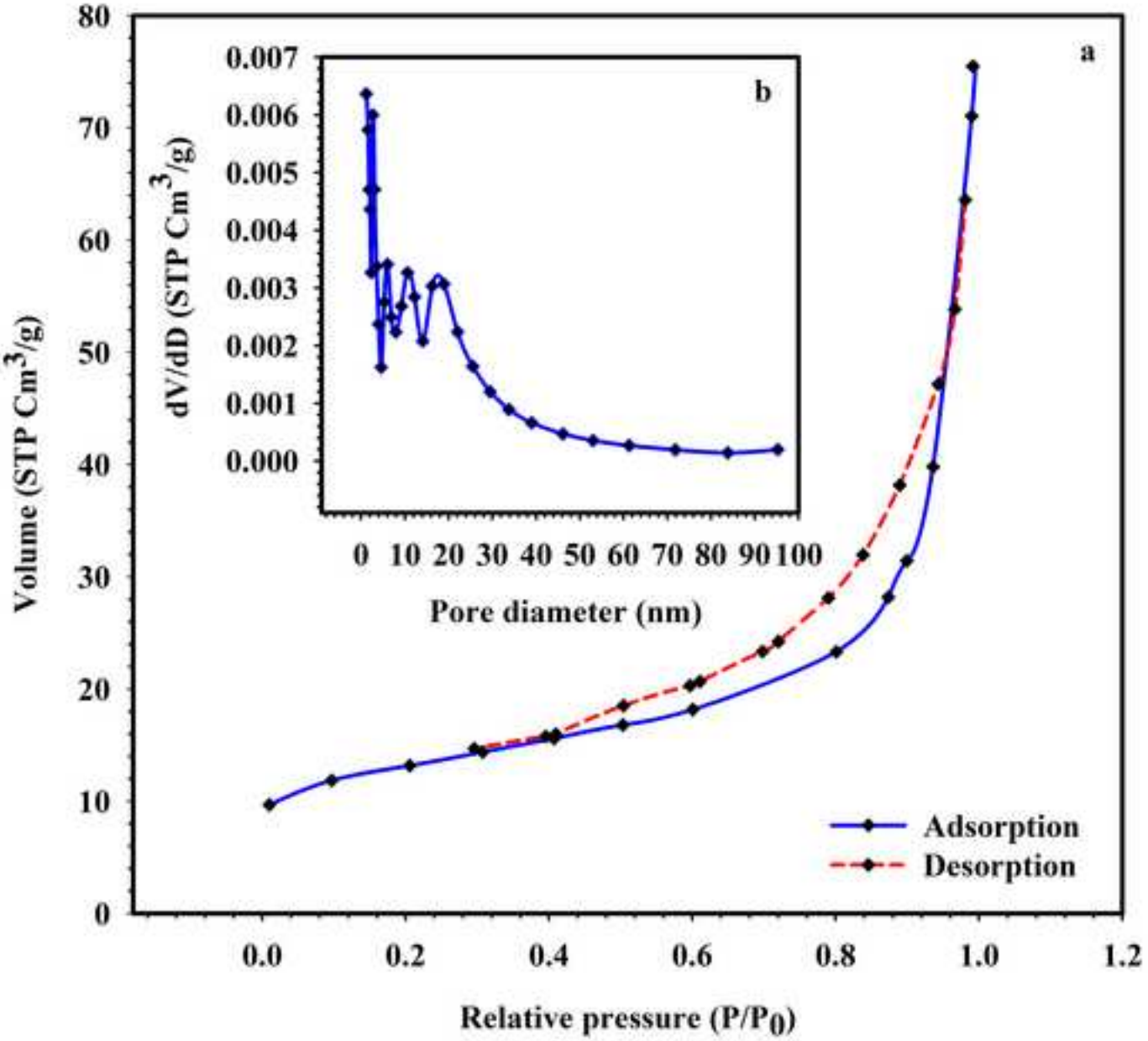

Fig. 6

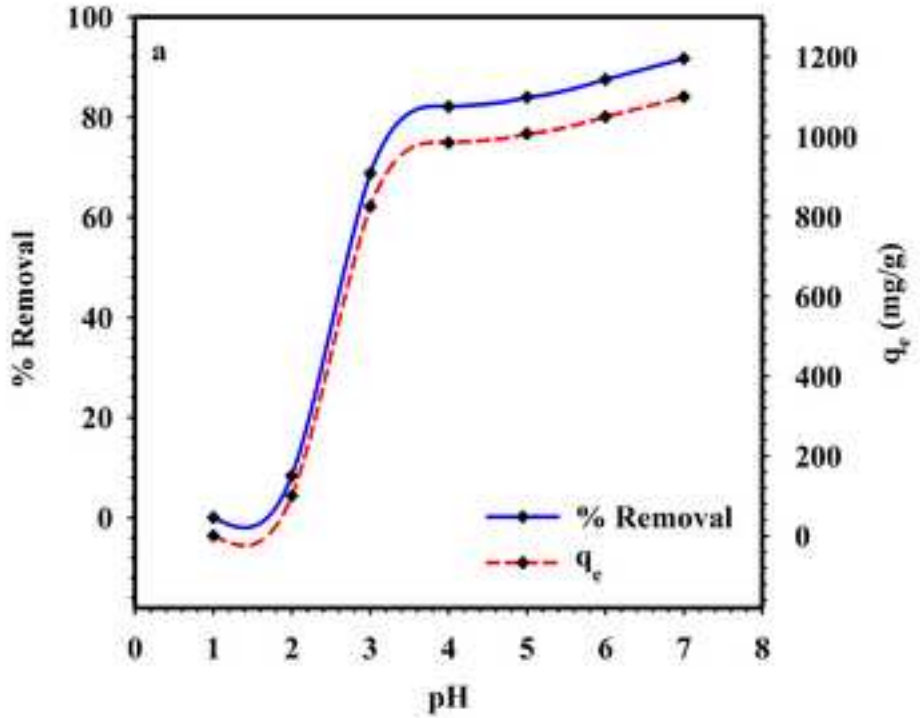

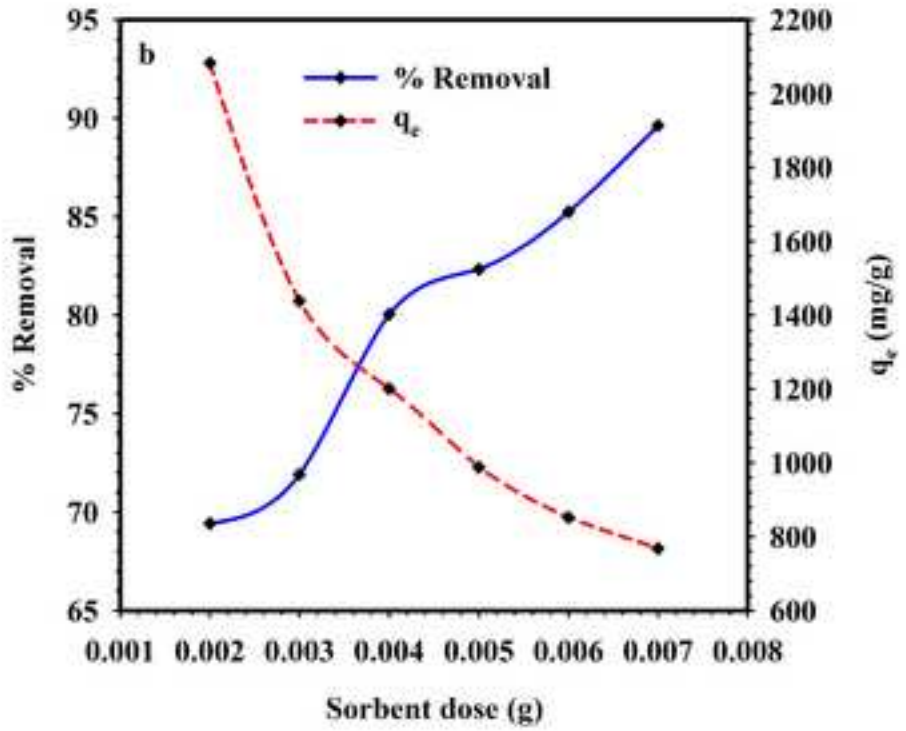

Fig. 7

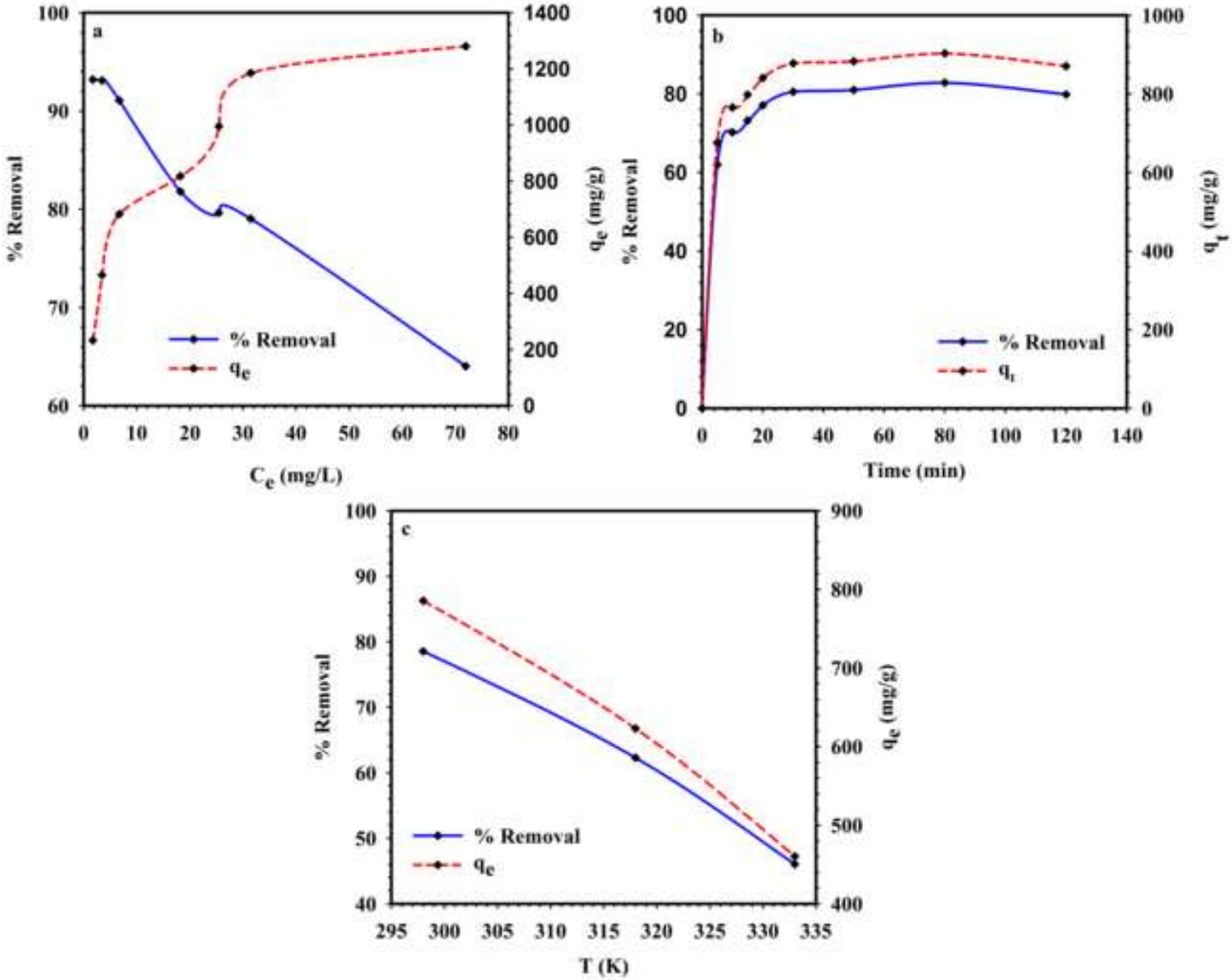

Fig. 8

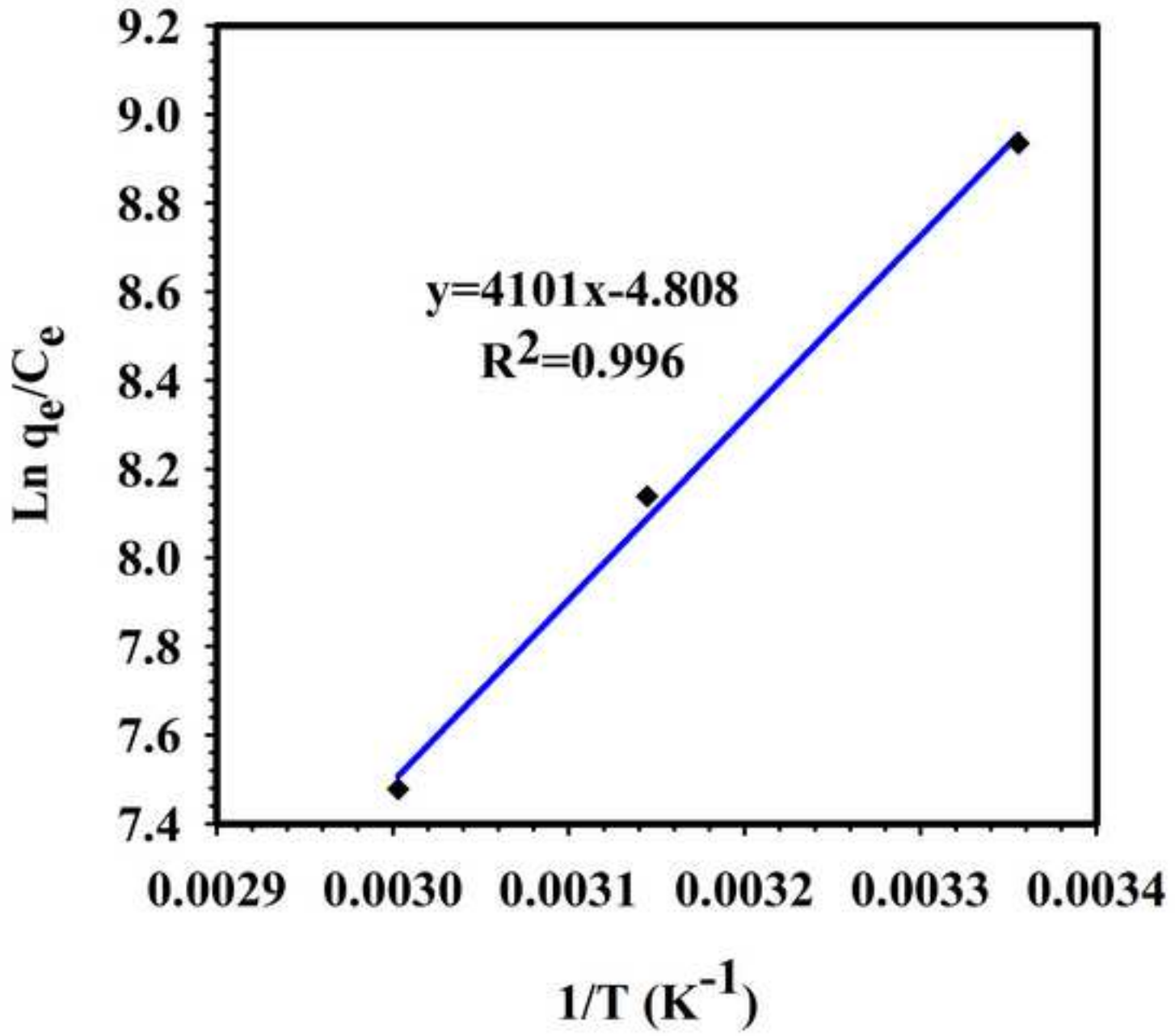

Fig. 9

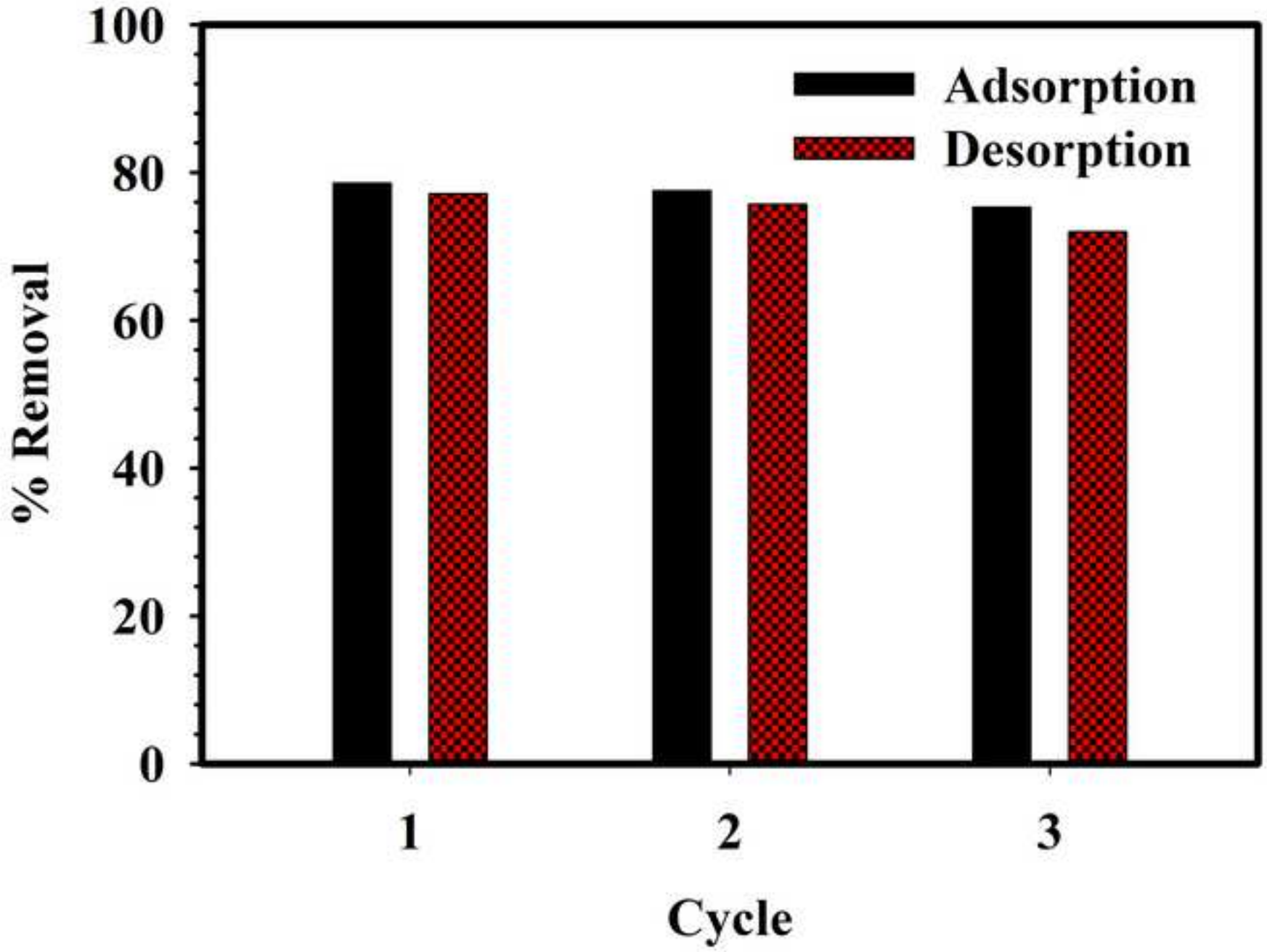

Fig. 10

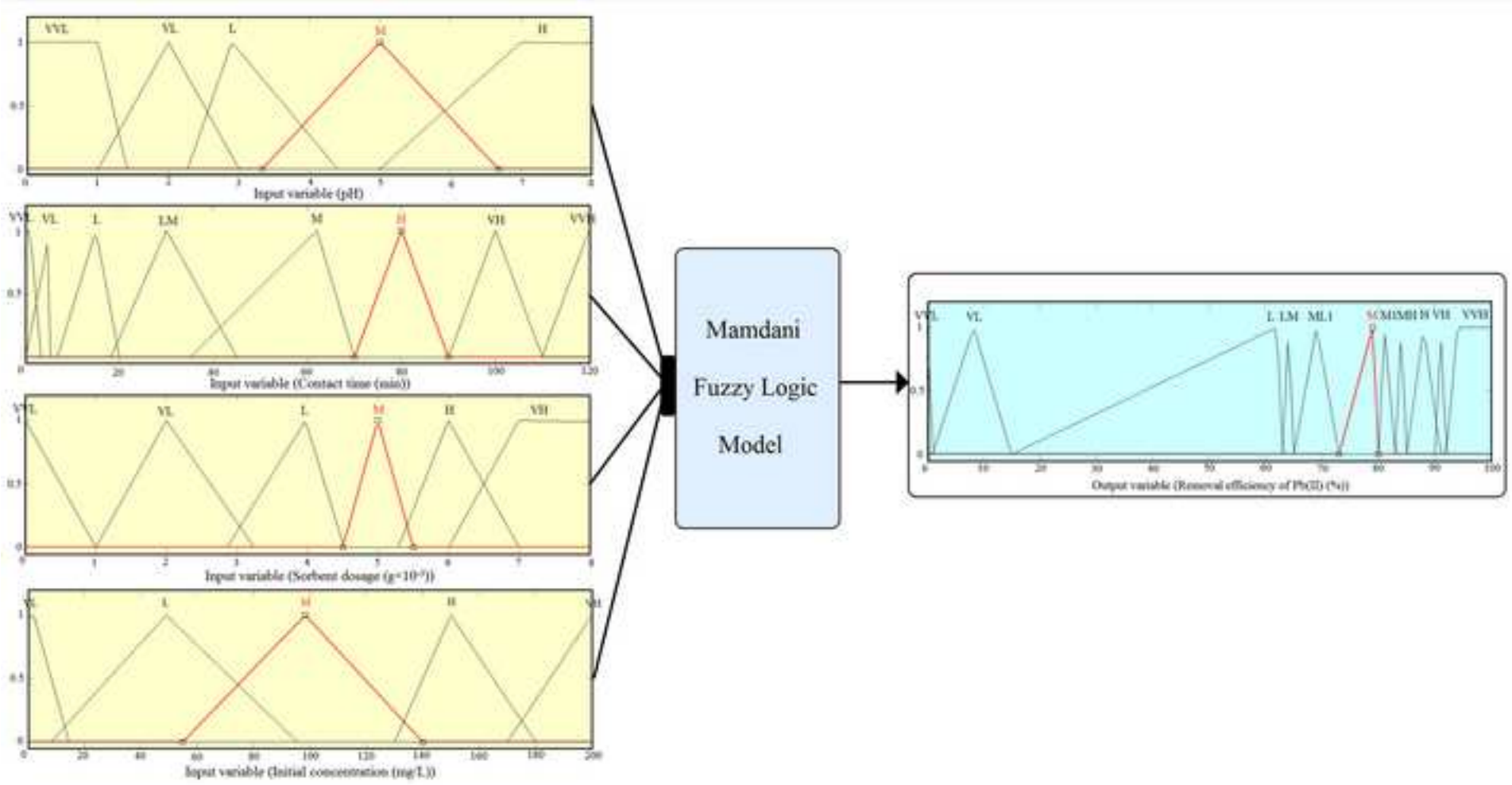

Fig. 11

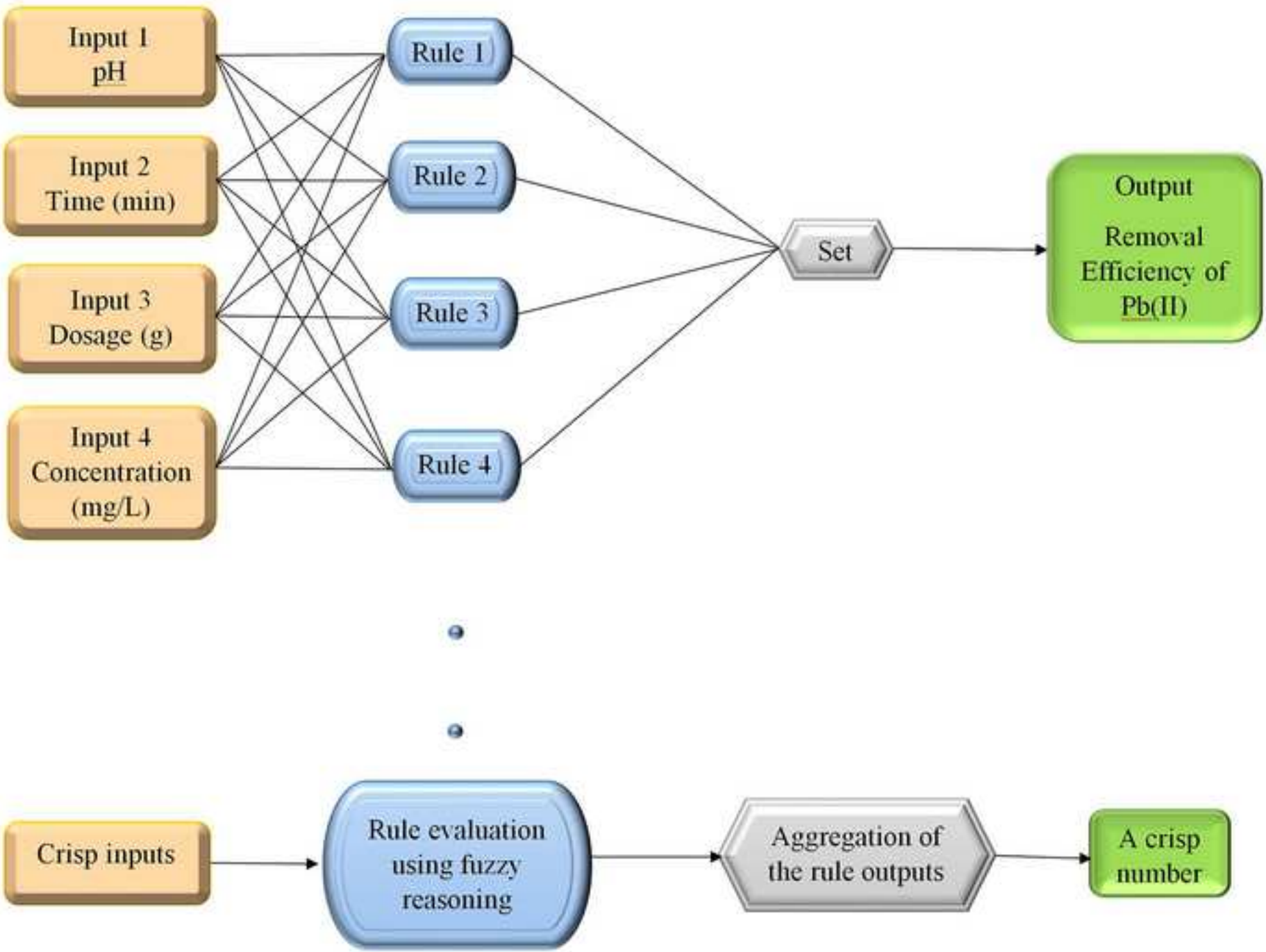

Fig. 12

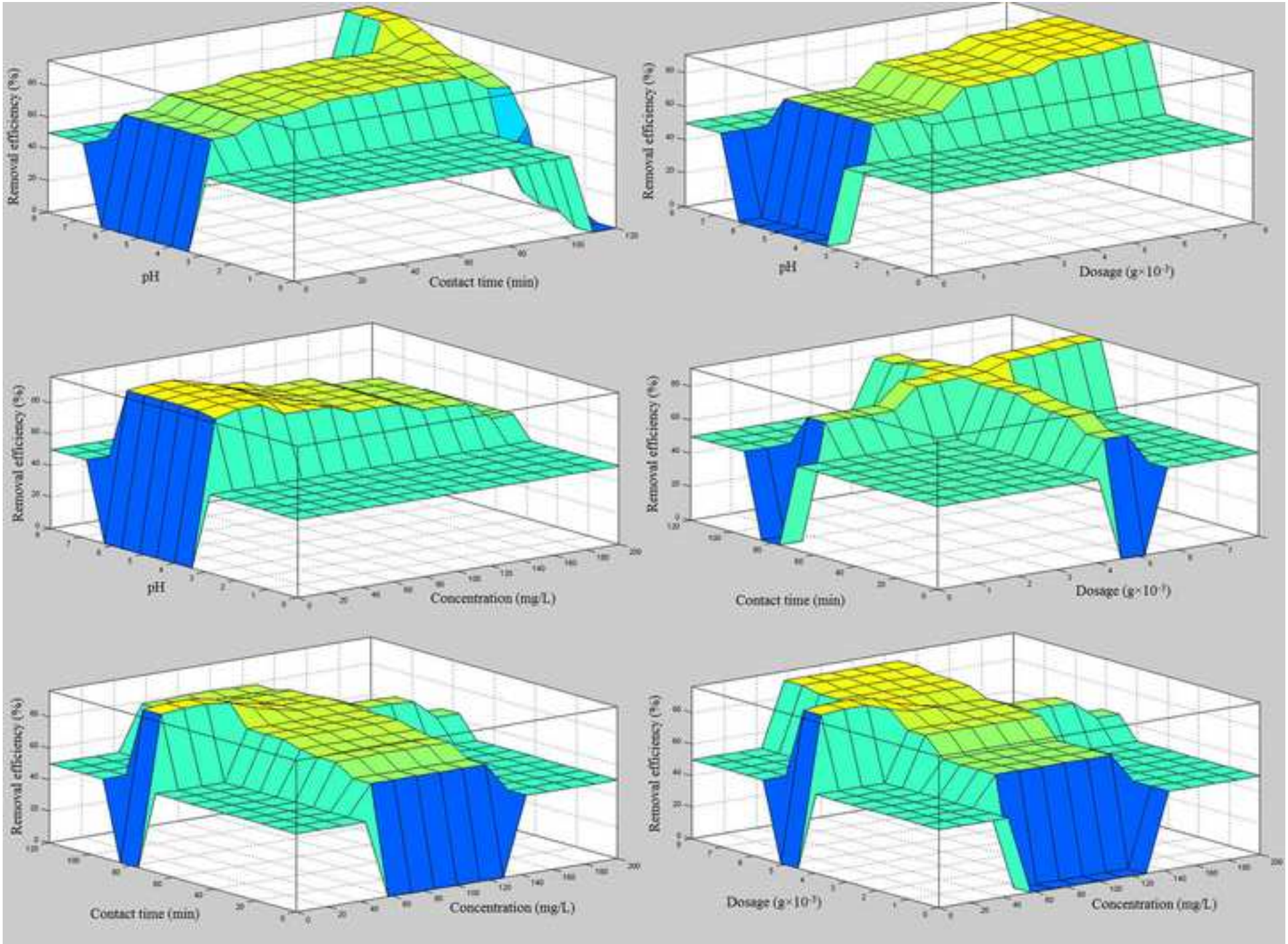

Fig. 13

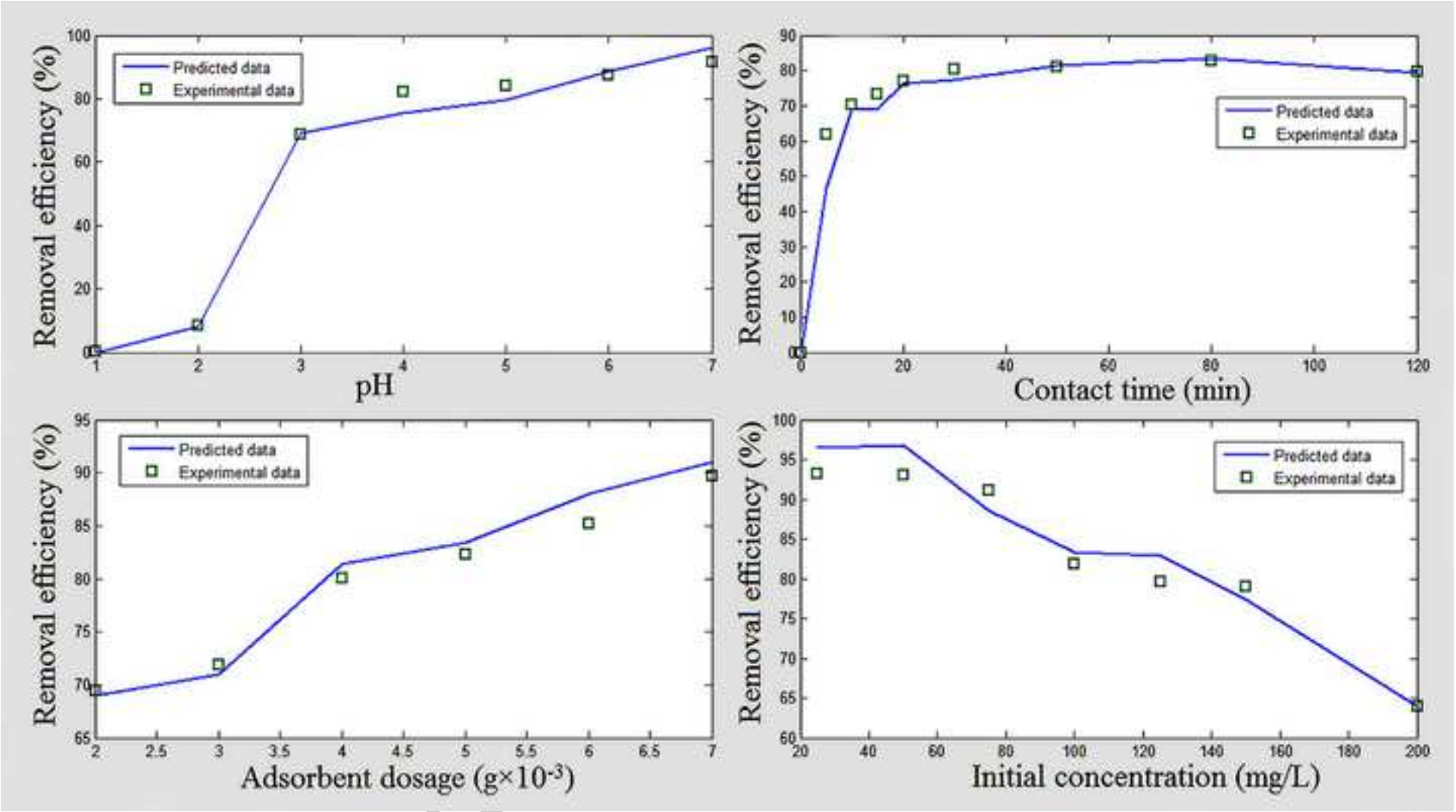

Fig. 14

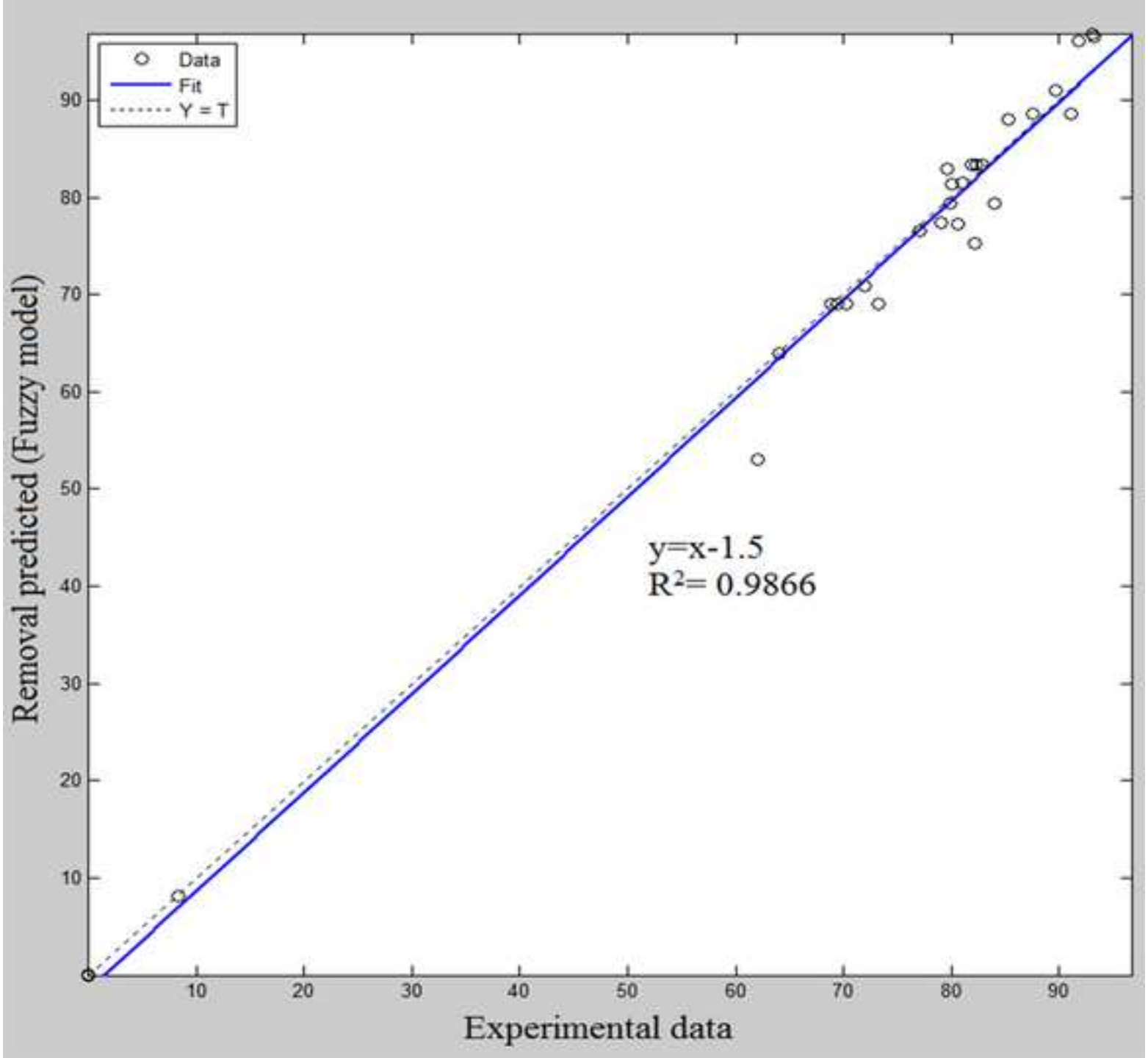

Fig. 15

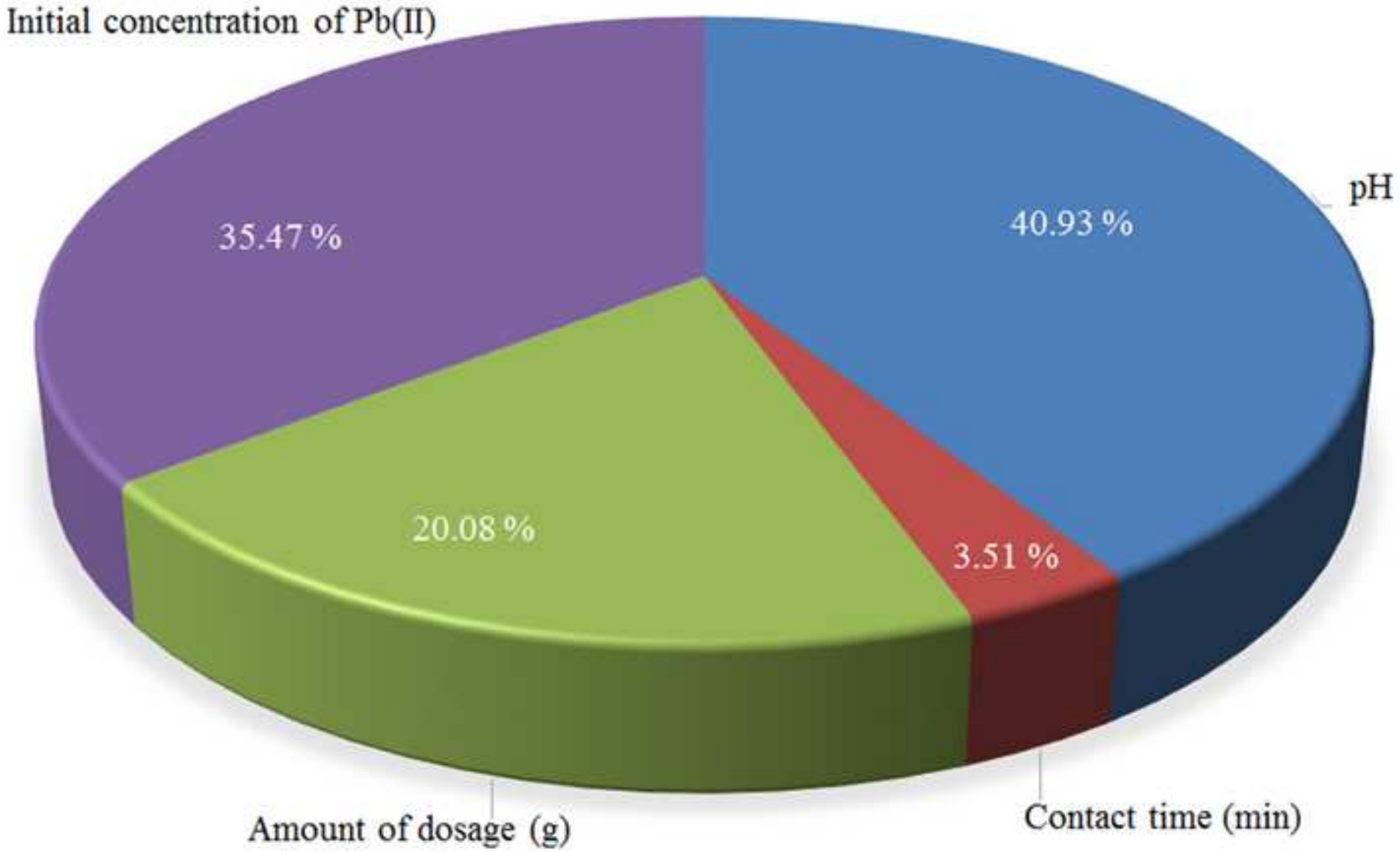

Table 1. Surface area and pore analysis of NiO/ACNC.

S_{BET} (m^2/g)	47.178
V_{BET} (cm^3/g)	10.839
S_{BJH} (m^2/g)	0.0264
V_{BJH} (cm^3/g)	0.1005
$V_{p,total}$ (cm^3/g)	0.1108
$d_{p,av}$ (nm)	9.3906

Table 2. Adsorption isotherms of Pb (II) ions

Model		Parameter	Values
Langmuir	Type 1	K_L (L/mg)	0.109
		q_m (mg/g)	1428.571
		R^2	0.986
		R_L	0.098
	Type 2	K_L (L/mg)	0.118
		q_m (mg/g)	1428.571
		R^2	0.983
		R_L	0.091
	Type 3	K_L (L/mg)	0.142
		q_m (mg/g)	1315.8
		R^2	0.882
		R_L	0.078
	Type 4	K_L (L/mg)	0.125
		q_m (mg/g)	1383.770
		R^2	0.882
		R_L	0.070
Freundlich		K_F	239.883
		$1/n_F$	0.433
		R^2	0.918
Temkin		K_T	0.369
		B	281.39
		B ln K_T	103.88
		R^2	0.969

Dubinin-Radushkevich	K_D	1.161
	Q_m	968.356
	E	0.656
	R^2	0.873

Table 3. Adsorption kinetics of Pb (II) ions

Model		Parameter	Initial concentration (mg/L)	
			50	100
Pseudo-first-order		$q_{e(exp)}$ (mg/g)	442.5	925.5
		q_e (mg/g)	184.671	202.162
		k_1 (min -1)	0.026	0.019
		R^2	0.884	0.474
Pseudo-second-order	Type 1	$q_{e(exp)}$ (mg/g)	442.5	925.5
		q_e (mg/g)	434.782	909.090
		k_2 (g/mg.min)	0.001	0.00006
		R^2	0.998	0.999
	Type 2	q_e (mg/g)	416.666	909.090
		k_2 (g/mg.min)	0.0008	0.00006
		R^2	0.981	0.973
	Type 3	q_e (mg/g)	427.84	908.68
		k_2 (g/mg.min)	0.00007	0.00006
		R^2	0.965	0.958
	Type 4	q_e (mg/g)	429.990	912.199
		k_2 (g/mg.min)	0.0007	0.0005
		R^2	0.965	0.958
Intra particle diffusion		K_i (mg/g.min)	31.56	59.191
		I (mg/g)	163.3	431.1
		R^2	0.663	0.501
Elovich model		α (mg/g.min)	1.253	1.345
		β (mg/g)	83.448	166.41
		R^2	0.874	0.747

Table 4. Thermodynamic parameters for the adsorption of Pb (II) ions

ΔH° (kJ/mol)	ΔS° (kJ/mol.K)	ΔG° (kJ/mol)		
		25 °C	45 °C	60 °C
-34.098	-0.0399	-22.135	-21.517	-20.703

Table 5. Comparison of the maximum monolayer adsorption (q_m) of Pb (II) onto various adsorbents.

Adsorbent	S_{BET} (m^2/g)	q_m (mg/g)	Reference
Iron-oxide nano-particles-immobilized sand	–	2.087	[64]
Iron oxide nanoparticles immobilization of *Phanerochaete chrysosporium*	–	185.25	[65]

Hierarchical calcium carbonate	63.2	3242.48	[67]
Magnetic alginate beads based on maghemite nanoparticles	–	50	[68]
Amino-functionalized magnetic nano-adsorbent	–	40.10	[69]
Polymer-modified magnetic nanoparticles	–	166.1	[70]
Magnetite nanoparticles	125.77	3.44	[71]
Chitosan/magnetite nanocomposite beads	–	63.33	[72]
Nano zerovalent iron nanoparticles graphene composite	–	585.5	[73]
Fe_3O_4@SiO_2–NH_2 nanoparticles	138	361.01	[74]
Iron oxide nanoparticles immobilized *Phanerochaete chrysosporium*	–	176.33	[75]
Amine-functionalized mesoporous Fe_3O_4 nanoparticles	25.94	369.0	[76]
Magnetic carbonaceous nanoparticles	60.0	123.1	[77]
Iron oxidenanoparticles	43	36.0	[78]
NiO/ACNC	47.178	1428.57	This study

Table 6. Experimental data and predicted response of fuzzy logic model for removal efficiency of Pb(II) (%) along with four independent variables.

Run order	pH	Contact time	Dosage	Concentration of	Removal efficiency of Pb(II) (%)

		(min)	($g \times 10^{-3}$)	Pb(II) (mg/L)	Experimental data	Fuzzy logic
1	1	120	5	100	0.0416	0.0407
2	2	120	5	100	8.3750	8.0061
3	3	120	5	100	68.7910	69.0000
4	4	120	5	100	82.1250	75.3251
5	5	120	5	100	84.0000	79.4051
6	6	120	5	100	87.5410	88.6322
7	7	120	5	100	91.7080	96.0512
8	5	0	5	100	0	0.0011
9	5	5	5	100	61.9720	53.0000
10	5	10	5	100	70.2290	69.0000
11	5	15	5	100	73.2110	69.0000
12	5	20	5	100	77.1100	76.5000
13	5	30	5	100	80.5500	77.3137
14	5	50	5	100	81.0090	81.4744
15	5	80	5	100	82.8440	83.3795
16	5	120	5	100	79.8620	79.4051
17	5	80	2	100	69.4160	69.0000
18	5	80	3	100	71.9160	70.9334
19	5	80	4	100	80.0410	81.3457
20	5	80	5	100	82.3330	83.3795
21	5	80	6	100	85.2500	88.0000
22	5	80	7	100	89.6280	91.0000
23	5	80	5	25	93.2000	96.5000

24	5	80	5	50	93.1000	96.7276
25	5	80	5	75	91.0660	88.6181
26	5	80	5	100	81.8000	83.3795
27	5	80	5	125	79.6400	82.8829
28	5	80	5	150	79.0330	77.3333
29	5	80	5	200	64.0250	64.0000

Table 7. MSE, RMSE, ARE, AARE and SD for removal efficiency of Pb(II) modeled by Fuzzy logic.

Response variable	Method	MSE	RMSE	% ARE	% AARE	% SD	R^2
Removal efficiency (%)	Fuzzy	8.9036	2.9839	0.89	2.87	2.99	0.9866

Table 8. Comparison between the current work and other performed models on removal efficiency of various adsorbents.

Adsorbents	Method	Response variable	Statistical index	Ref.
Active carbon (AC)	ANN	Pure and binary gas absorption	R^2= 0.997	[79]
ZnS nanoparticle loaded on AC	ANN-PSO MLR	BG dye removal	$R^2_{ANN-PSO}$= 0.9610 R^2_{MLR}= 0.9231	[80]
AC	ANN	SY dye removal	R^2= 0.998	[81]
ZnS nanoparticles loaded on AC	ANN $RSM_{(CCD)}$	BG and EB dyes removal	R^2_{ANN-BG}= 0.9589 R^2_{ANN-EB}= 0.9455 R^2_{CCD-BG}= 0.9645 R^2_{CCD-EB}= 0.9527	[82]
Cu nanowires loaded on AC	ANN, MLR	Malachite green (MG) removal	R^2_{ANN}= 0.9658 R^2_{MLR}= 0.8133	[83]
AC	$RSM_{(CCD)}$	4-CP removal	R^2= 0.949	[84]
Fe_2O_3–ZnO–$ZnFe_2O_4$/ carbon nano-composite	$RSM_{(CCD)}$	BPB dye removal	R^2_{CCD}= 0.9947	[85]
SnS-NP-AC	RF	CR dye removal	R^2= 0.9793	[86]
CuO–ZnO nano-Composite	GP	DR23, DR80 and DR81 dyes removal	R^2_{DR23}= 0.9837 R^2_{DR80}= 0.9616 R^2_{DR81}= 0.9763	[87]

(FCZN)				
NiO/ACNC	Fuzzy	Pb(II) removal	R^2= 0.9866	Current work

Highlights

- NiO/ACNC was prepared by sonochemical method.
- According to N_2 adsorption-desorption, mesoporous structure exists in sorbent.
- NiO/ACNC has high adsorption efficiency toward Pb (II).
- Adsorption process was controlled by pseudo-second-order equation.
- Removal efficiency of Pb (II) was predicted using the developed fuzzy logic model.